Final SBIR Phase I Report

Contract No: N00014-93-C-0154

"Control of Interface Properties of Light Metal Composites through In-situ Metallurgical Processing"

Research supported by the Ballistic Missile Defense Organization (Formerly Strategic Defense Initiative Office)/Innovative Science and Technology, managed by the Office of Naval Research

SDI SBIR Topic no. 93-013#2

Data Acquisition Document No. DI MISC-80508/M

Final Contract Report

September 2, 1994

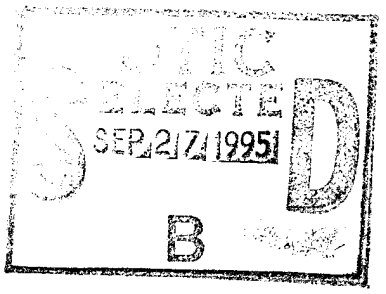

Prepared by:

Dr. James A. Cornie, Dr. Maxim L. Seleznev,
Mr. Shi-yu Zhang, and Mr. Mark A. Ryals

Metal Matrix Composite Castings, Inc. (MMCC, Inc.)
101 Clematis Ave. #1
Waltham, MA 02154
617-893 4449

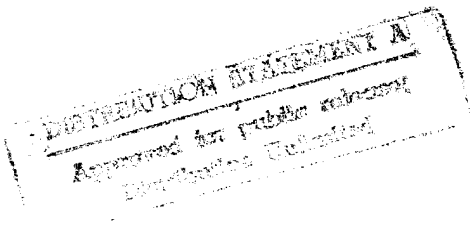

Attention:
Scientific Officer
Dr. Steven G. Fishman, Code 3313
800 North Quincy Street
Arlington, VA 22217-5660

DISCLAIMER NOTICE

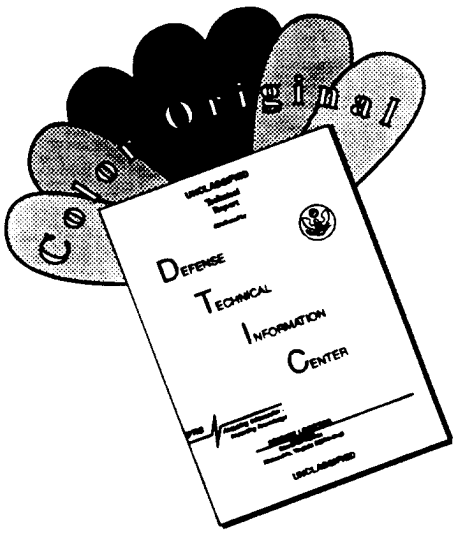

THIS DOCUMENT IS BEST QUALITY AVAILABLE. THE COPY FURNISHED TO DTIC CONTAINED A SIGNIFICANT NUMBER OF COLOR PAGES WHICH DO NOT REPRODUCE LEGIBLY ON BLACK AND WHITE MICROFICHE.

Final SBIR Phase I Report

Contract No: N00014-93-C-0154

"Control of Interface Properties of Light Metal Composites through In-situ Metallurgical Processing"

Dr. James A. Cornie, Dr. Maxim L. Seleznev
Mr. Shi-yu Zhang and Mr. Mark A. Ryals

Table of Contents

List of Figures

List of Tables

Final SBIR Phase I Report

Contract No: N00014-93-C-0154

"Control of Interface Properties of Light Metal Composites through In-situ Metallurgical Processing"

Dr. James A. Cornie, Dr. Maxim L. Seleznev,
Mr. Shi-yu Zhang, and Mr. Mark A. Ryals

1.0 Introduction and Summary of Results

1.1 Introduction

The properties of continuously reinforced aluminum composites have been notoriously unpredictable and prone to extreme scatter. Early results from MIT studies that preceded this study showed that matrix metallurgy was important in yet to be understood ways. As MMCC and MIT researchers working in collaboration investigated the phenomena, we discovered that controlled equilibrium precipitation on the fiber surface could be used to control interfacial delamination, long recognized as necessary for toughening of continuously reinforced metal matrix composites. This report summarizes our present understanding of this phenomena and points the way toward applying deep metallurgical understanding to the use of commercial alloys to optimize the mechanical behavior of continuously reinforced MMCs.

It can fairly be stated that the most important impediment to the application of MMCs, aside from cost, is the non-uniformity and unpredictability of mechanical properties. The designer may accept Weibull statistical design principles for a small ceramic part; however, he will insist that metal matrix composites have the uniformity in properties a metal and that components can be similarly designed with design minimums. The cost issue will be met head-on by adopting near-absolute net shape processing as used in this study. The predictability and reliability issue, however, is related to our ignorance of the effects of matrix metallurgy on the mechanical behavior of composites. When we have understood the interaction between matrix metallurgy and near-absolute net-shape cast processing, we will have placed behind us the chief impediments to large scale application of this exciting class of materials.

This program focused on matrix metallurgy. We have succeeded in stating the most important fundamental principles governing the mechanical behavior of continuously reinforced Al alloys. The Phase II continuation will be focused on refining the composition ranges and heat treatment conditions of the more notable systems identified here, developing a data base for these systems, and extending the study to the case of discontinuously reinforced Al alloys (which are likely to economically more important).

1.2 Summary

Axial strengths in Nextel 610™ (alumina fiber) reinforced aluminum alloys are optimized in systems with high solubility and where equilibrium precipition occurs with a work of adhesion to the fiber less than the work of adhesion to the matrix. The θ precipitate (Al_2Cu) is a model example. Similar effects are also noted in the ternary system Al-Mg-Zn. The transverse strength of composites is enhanced by strong bonding. The degree of bonding can be varied by controlling the precipitation extent on the fiber matrix interface by controlled aging heat treatments and by ternary additions that increase adhesion by introducing more strongly adherent precipitates to dilute the effect of weakly adherant precipitates. A good example of such a system is the Al-Cu-Si system which contains both strongly adherant Si and weakly adherant θ precipitates at the interface.

1.3 Conclusions

We believe we have tapped into a gold mine of possibilities for optimization of both continuously reinforced Al matrix composites (in both axial and transverse directions) and discontinuously reinforced composites and are within reach of having the ability to specify alloy chemistry and heat treatments for the control and optimization of MMC mechanical behavior. We conclude that we do not need to invent new alloys to optimize composite behavior. Rather, we must find existing alloys in the important ternary and binary systems that, with judicious control of matrix chemistry and proper heat treatment, can be used to optimize the mechanical behavior of continuously and discontinuously reinforced aluminum alloys. We have done our prospecting. However, most of the gold is still in the mine and must be removed to the smelter and refined. This will be left to the alchemy of Phase II.

2. 0 Goals of the SBIR Research

The main goal of this research was to explore the possibilities of using different aluminum alloys as matrix material for aluminum/alumina composite. The candidate alloys were chosen from base commercial systems potentially capable of producing discontinuously intermetallic precipitate coated interfaces (DCI) between the fiber and the matrix[1,2].

This goal was coupled with the technological task of testing the new version of pressure infiltration technology where the evacuation and melting stage was separate from the infiltration and solidification. These alloy studies, however, will have general applicability to all continuously reinforced Al alloy composites.

---

[1]Cornie, J.A., M.L. Seleznev, M. Ralph and F.A. Armatis, Jr., "Improving mechanical properties of Nextel 610 reinforced Al-224 alloy through θ phase precipitation at the fiber-matrix interface, Materials Science and Engineering A162 (1993) 135-142.

[2]Seleznev, M.L., J.A. Cornie, and F.A. Armatis, Jr., "Improving Mechanical Properties of Nextel 610™-Reinforced Al-224 Alloy through θ Phase Precipitation at the Fiber/Matrix Interface: Kinetics of the Precipitation Process, JMEPG (1993) 2:347-352.

Indeed, this work and the Phase II effort that grows out of this work will be necessary for the full realization of the structural potential of these systems.

3. 0 Experimental Methods and Procedures

3.1. Alumina fiber used for production of metal matrix composites

In research presented here, we used as reinforcement the Nextel 610™ sol-gel derived, continuous polycrystalline alumina fiber commercially available from 3M Corporation. A fiber characterization study yielded the diameter distribution shown in Figure 3.1 and the cumulative strength distribution shown in Figure 3.2. The average strength of the fiber varied between 1.5 and 2.5 GPa from spool to spool. The fiber diameters vary between 10 and 15 μm within a single tow. Application of the Weibull statistics procedures described in detail elsewhere yielded a Weibull modulus of approximately 4.5 for this fiber. This low modulus represents a wide cumulative strength distribution as compared to more developed fibers, such as boron, which is characterized by a Weibull modulus of 15.

3.2. The choice of the matrix alloys and heat treatment regimes

In earlier studies[1,2] we used the Al-224.2 commercial alloy as a matrix material. We expanded this study to include other interesting matrix systems. The compositions, heat treatments and expected precipitating phases for the alloys used in the study are presented in the Table 3.1

Table 3.1 Candidate Alloys Compositions, Heat Treatments and Expected Precipitating Phases

System	Com-position.	Heat Treatment	Precipitating phases	Ref. Figs
Al-Cu-Mg*	4.5% Cu 1.5%Mg; Balance Al	495C, 24h + water quench. + 200C, 4h + annealing at 350C and 400C for 1,3,10,30 and 100 hours	$CuMgAl_2$	Figure 2.1
Al-Cu-Si**	4.5%Cu; 1.2%Si; Balance-Al	515C, 24 h + water quench + 200C, 4h + 400C ,48h	$CuAl_2$, Si	Figure 2.2
Al-Mg*	9.1%Mg; Balance Al	400C, 48h + water quench + 200C, 4h + annealing at 300C for 1,3,10,30 and 100 hours	Mg_3Al_2	Figure 2.3
Al-Mg-Zn**	5%Zn; 9.5%Mg; Balance Al	440C, 48h + water quench. + 200C, 2h + 300C, 48h	$Mg_3Zn_3Al_2$	Figure 2.4
Al-Si**	5%Si; balance-Al	565C, 24h + water quench + 200C, 4h + 350C, 48h	Si	Figure 2.5

*- an old pressure infiltration technology was used to produce composite (see § 3.3)
**- the new MMCC technology was used to produce composite (see § 3.3)

3.2.1. Background for the choice of alloys and heat treatments

3.2.1.1 Al-Cu-Mg system

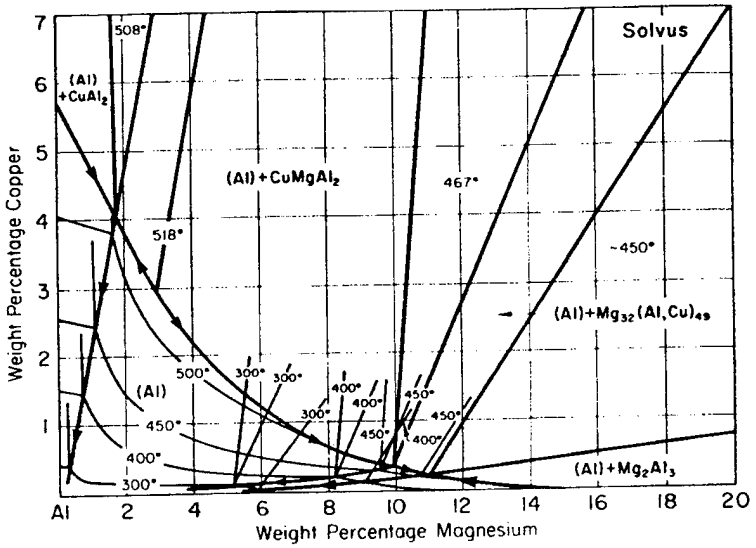

Figure 3.3 Al-Cu-Mg phase diagram

We may expect precipitation of $CuMgAl_2$ phase at the interface (Figure 3.3) for the alloys of the Al-Cu-Mg system. The addition of magnesium could possibly increase the precipitation density at the interface compared to binary Al-Cu alloy. A potential problem with Mg reactivity was expected and the investigation confirmedthis problems existence for alloys at lower magnesium concentrations, (~1.5%) but not at high Mg levels (>5%).

3.2.1.2 Al-Cu-Si system

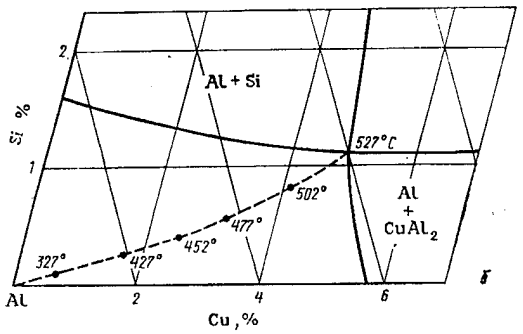

Figure 3.4 Al-Cu-Si phase diagram.

The main reason for studying this system was the possibility of increasing the area fraction of submicron brittle particles at the interface. This goal was achieved by alloying the Al-Cu system with Si. Practically all silicon is expected to first dissolve in the matrix during homogenization and then precipitate in the form of fine particles after annealing. As in case of Al-Cu one may expect enhanced precipitation at the fiber-matrix interface. Judging from weight

fraction of Si in the alloy, the area fraction of fiber surface covered with precipitates may increase from about 20% in case of Al-4.5% Cu alloy to over 30% for Al-4.5%Cu-1.2%Si. The increase of area fraction covered with precipitates, however, will not be accompanied by an increased presence of brittle eutectic constituents in the structure of the matrix alloy since all of the Si added will be dissolved during homogenization treatment.

3.2.1.3 Al-Mg system

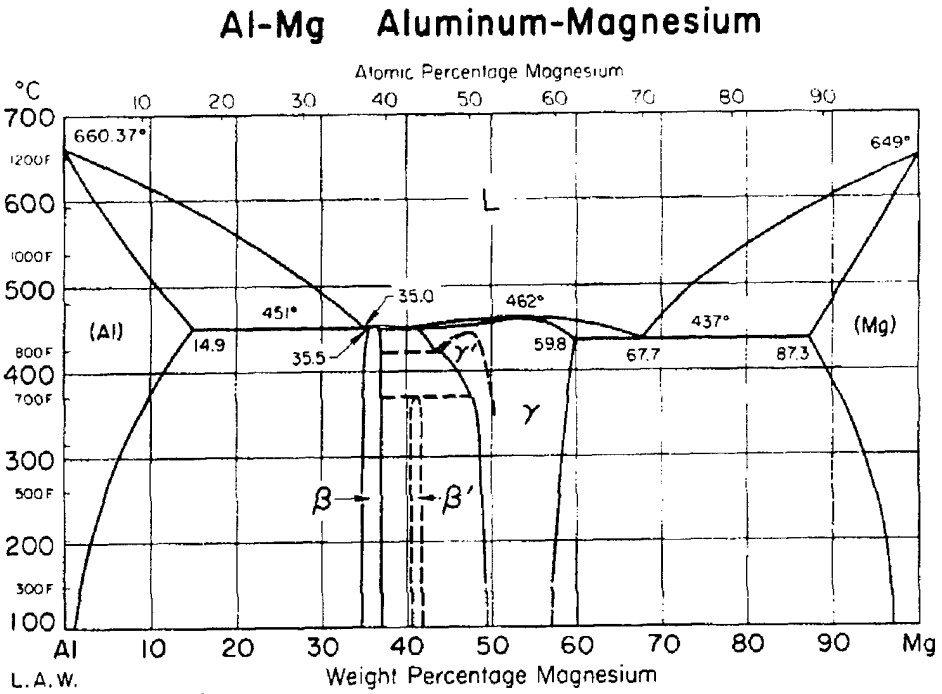

Figure 3.5 Al-Mg phase diagram.

The high concentration of Mg in the chosen alloy guarantees a very high precipitation density at the fiber-matrix interface. As in the case of Al-Cu-Mg alloy there is a potential Mg reactivity problem. Another unclear issue is how the Mg-rich phases adhere to alumina substrates. Mg in Mg_3Al_2, unlike Cu in $CuAl_2$, might increase the adhesion to alumina as compared to pure aluminum adhesion. Data on this subject is not available.

3.2.1.4 Al-Si system

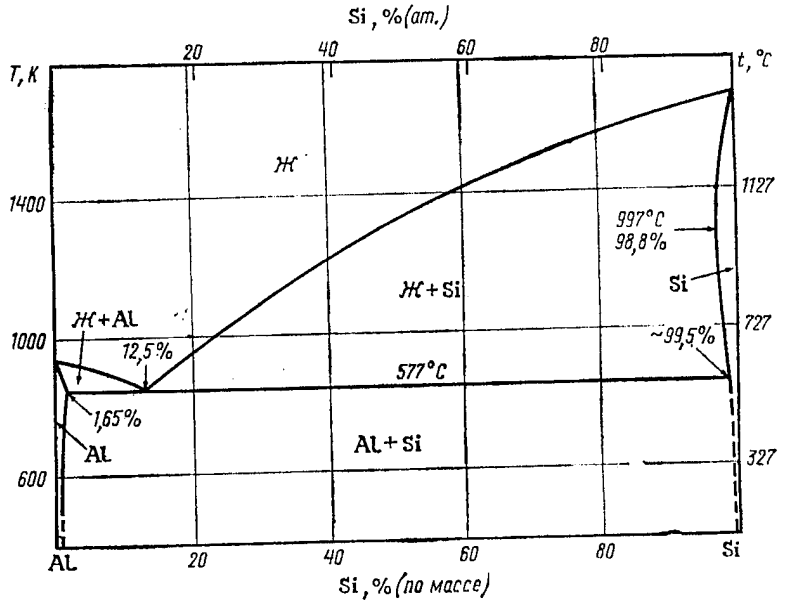

Figure 3.6 Al-Si phase diagram

The Al-Si system may be a successful candidate for the DCI effect for two reasons: The first reason is that up to 1.65% Si may be dissolved in aluminum solid solution during homogenization and then precipitated upon annealing. The second reason is that eutectic silicon may be easily spheroidized during homogenization at high temperature. During solidification of cast composites the growing primary aluminum rich dendrite will reject solute ahead of the solidifying dendrite to the fiber interface [3] and to interdendritic regions. Thus, the interface region will be enriched with a material approaching the Al-Si eutectic composition. Upon homogenization the needles of eutectic silicon, many of which will be at the interface, are expected to spherodize. Si precipitation will drastically increase the area fraction of brittle islands at the interface. The important question to be answered experimentally is: what is the size of the spherodized particles of eutectic silicon and how can we control their growth? If their size is substantially higher than 1 μm, then they may decrease composite strength by serving as a crack initiator.

[3] Mortensen, A., Cornie, J.A., and Flemings, M.C.; "Columnar Dendritic Solidification in a Metal-Matrix Composite", Metallurgical Transactions A, 19A, pp. 709-721, (1988).

3.2.1.5 Al-Mg-Zn system

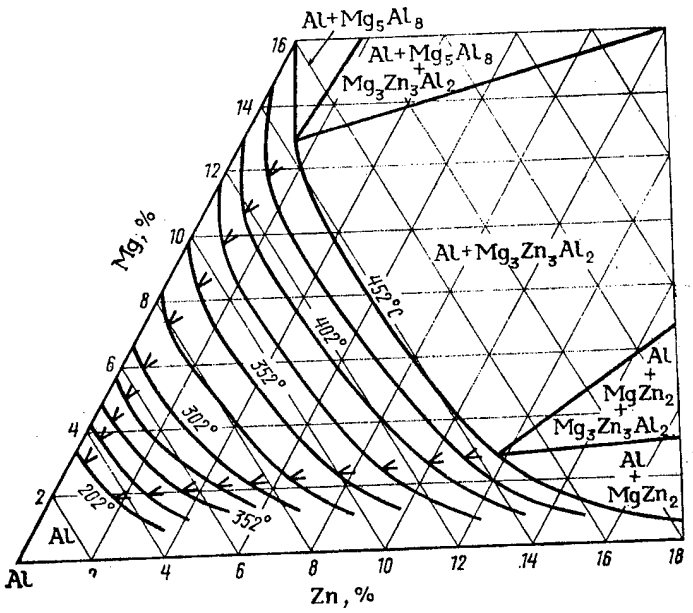

Figure 3.7 Al-Mg-Zn phase diagram

The alloys of this system are some of the strongest aluminum alloys at room temperature due to intensive precipitation reactions. The only potential problem when using this system as DCI alloys is reactivity of Mg with alumina fiber. In this system we can expect very intensive interfacial precipitation of T-phase ($Mg_3Zn_3Al_2$). Whether this phase is adhering to alumina loosely enough to cause the DCI effect should be a matter of investigation.

3.3 Infiltration technology used for composite specimen production†

Two different technologies were used to produce the alumina fiber/aluminum alloy composites. The first technology is the same as used in earlier studies.[1,4] In this scheme shown in Figure 3.8 the preform evacuation, metal melting and finally infiltration of the preform by the molten metal takes place in the same vessel. An electric resistance furnace was used to melt the metal and heat the preform. By this technology we produced composites with Al-Cu-Mg and Al-Mg matrices.

The technology being developed at **MMCC, Inc.** abandoned that approach. In our version of the technology the evacuation of the preform and melting of the metal takes place in one vessel, and pressurization and infiltration of the preform by the molten metal in another as shown in Figure 3.9. Induction heating is used to melt the metal. This enables us to produce even the nickel matrix composites. We

---

† **Section 3.3 is considered to be proprietary to MMCC, Inc. The remainder of this document may be openly quoted.**

[4] Mortensen, A., Masur, L.J., Cornie, J.A., and Flemings, M.C., "Infiltration of Fibrous Preforms by a Pure Metal, Part 2: Experiments," Metallurgical Transactions A, 20A, pp. 2549-2557, (1989)

produced composites with Al-Mg-Zn, Al-Cu-Si and Al-Si matrices for this program using this technology.

Because of the high power rating of the induction furnace it was easy to overheat the melt. This was not a problem for the older, much slower electrical resistance heated machines. The mold vessel we use for production of the composites is a low carbon steel can with metal contact surfaces coated with colloidal graphite. We experienced iron contamination in a number of castings, due in part to excessive superheat and, in part, to insufficient protection of the mold vessel afforded by the colloidal graphite coating. Fe contamination results in formation of extremely brittle (FeCuAl), $FeAl_3$ or (FeSiAl) phases shown in Figure 3.10. The presence of these phases in large quantities drastically reduces the strength of aluminum alloys and composites. The cracks initiated in these particles during cooling can easily penetrate the reinforcing fiber as shown in Figure 3.11. Further development of the technology; namely introduction of more precise temperature control and the development of a denser mold wash/reaction barrier should eliminate these problems in the future. This feature of the processing will be evaluated in detail in Phase II.

4. 0 Results and Discussion

4.1. Interface Precipitation and Coarsening Phenomena Study Results

4.1.1. Summary of earlier results for Al-Cu matrix composite.

4.1.1.1 Observations

Originally the phenomenon of enhanced precipitation at the interface which was related to an increase in mechanical properties, was observed in composite material annealed at 350C for several hours after the standard T7 heat treatment[1]. The microstructure of that composite is presented in Figure 4.1 In order to observe precipitation at the fiber/matrix interface in SEM we introduced the "diving fiber" technique. A schematic of the method is presented in Figure 4.2 Another option is to observe the precipitates at the interface directly, looking through the transparent body of the fiber at the polished crossection using the optical light microscope as shown in Figure 4.3.

As it became clear from further investigation, enhanced precipitation at the interface was of the same nature as the well known phenomenon of the enhanced precipitation of a second phase at a high angle grain boundary. Figure 4.4 clearly demonstrates that point.

4.1.1.2 Kinetics of precipitation and coarsening

In order to control precipitation at the fiber/matrix interface and, through that, the properties of composites, one needs to determine the kinetics of the process. We studied the kinetics of precipitation and coarsening of $CuAl_2$ at the fiber-matrix interface at two temperatures; 350 and 400C as shown in

Figure 4.5. The coarsening kinetics follows a $t^{1/4}$ rate law for both precipitate size and interparticle distance[5], and coincides with the theoretical predictions[5,6].

4.1.1.3 Particle size distribution of $CuAl_2$ at the matrix-fiber interface

Experimental particle size distribution, however, does not correspond to and even contradicts the theoretical predictions.[5,6] In theory, the shape of particle size distribution during coarsening should look similar to one in Figure 4.6(a). Our results in Figure 4.6(b) consistently show that the shape of the particle size distribution is contrary to theory: the cut-off size is about 2.5 μm and the curve is shifted to the left, not to the right, even after prolonged exposures at 400C. The reason for the discrepancy remains unknown and is of theoretical interest.

In conclusion, as a result of this study we have a reliable tool for tailoring the microstructure at the interface to our design even though we do not fully understand the coarsening process.

4.1.2 Results obtained in the present interface precipitate coarsening study for different aluminum alloy matrix composites

4.1.2.1 Observations of interface microstructure in Al-Mg, Al-Mg-Zn, Al-Cu-Mg, Al-Cu-Si and Al-Si matrix composites

The structure of fiber-matrix interface in Al-9.1% Mg matrix composite responded strongly to heat treatment. Figure 4.7 shows that the precipitates cover approximately 40% of the interface surface. The average size of the precipitates on the interface appears to be slightly over 1 μm.

The Al-9.5%Mg-5%Zn matrix composite shows a similar response as shown in Figure 4.8; however, the precipitate size at the interface is larger, approximately 2 μm. This larger precipitate size, compared with Al-Cu systems, is consistent with the high diffusivity of Zn in solid aluminum. Although this particular composite casting was contaminated with iron, Fe contamination had little or no effect on the precipitation density, because neither Mg nor Zn are present in any significant amount in the iron containing phases.

The fiber-matrix interface in the Al-4.5%Cu-1.5%Mg matrix composite showed a rather sluggish response to heat treatment as demonstrated in Figure 4.9. Precipitates cover slightly more than 10 percent of the interface area. A possible reason is that Mg, essential for precipitation of the $CuMgAl_2$, was consumed by reaction with fiber surface.

In Al-4.5%Cu-1.2%Si matrix composite the goal of getting $CuAl_2$ and additional Si precipitates at the interface appears to be reached. As Figure 4.10 shows there are bright and dark particles present at the interface. The dark (gray) particles are Si as confirmed by energy dispersive X-ray microanalysis.

---

5 A.J. Ardell, "on the Coarsening of Grain Boundary Precipitates, Acta Metall., 20,(1972), 601-609.
6 Kirchner, H.O.K., "Coarsening of Grain-Boundary Precipitates, Metall. Trans., 2,(1971), 2861-2864.

The Al-Si composite was so heavily contamination by iron during processing that Si could not be found in the structure as a separate phase. (see Figure 3.8)

4.1.2.2 Kinetics Of Coarsening And Particle Size Distribution In Al-Mg and Al-Cu-Mg Composites

For Al-Mg and Al-Cu-Mg matrix composites we have studied the coarsening kinetics of interfacial precipitates. We have chosen these two composites because they represent the extremes - the former having the highest precipitation density and the latter the lowest.

The results of the study for Al-Mg matrix composite are shown in Figure 4.11. The results do not contradict the theoretical prediction that precipitate size change linearly with $t^{1/4}$ during the coarsening process at internal interfaces. It follows from the study that varying time of the exposure at 300C both sub- and super-micron size particles may be found at the interface. The shape of the typical particle size distribution during coarsening is shown in Figure 4.12. It is close to the theoretical shape postulated by Ardel. The average size of the particles is about 1 μm and the cut-off size is about 1.8 μm ignoring scatter at the higher end of the distribution.

The coarsening kinetics for Al-4.5%Cu-1.5%Mg composite are shown in Figure 4.13. The results of kinetic studies at 350C are quite satisfactory from the point of view of the theory. The linear fit of size vs. $t^{1/4}$ is good. The 400C results show considerable scatter, which is probably due to a more severe reaction of Mg with the fiber at this temperature. The particle size distribution, even after 100h at 350C, is less then perfect as shown in Figure 4.14. The distribution maximum is shifted towards the smaller particle sizes and the cut-off size is about 2.5 instead of 1.5 as predicted by theory.

5.0 Mechanical Properties Of Composites Subjected To Heat Treatments Producing Controlled Interfacial Precipitation

5.1. Al-Cu matrix composite: summary of results

Measured mechanical properties are summarized in Figure 5.1. The Al-Cu matrix composites benefit enormously from interfacial precipitation when compared with as-cast and T7 heat treatments. However, maxima in tensile strength comes at the expense of transverse strength. Prolonged heat treatments result in a more favorable combination of the longitudinal and transverse strength.

The corresponding fracture surfaces for composites, with and without interfacial precipitation, differ strikingly. Highly irregular fracture with copious debonding for a composite with interfacial precipitation is noted in Figure 5.2 (a). This is contrasted to planar fracture surface for T7 heat treatment as shown in Figure 5.2 (b).

The fractographs of long time thermally exposed transverse specimens (that resulted in the strongest axial properties) reveal clean fracture surfaces. T7 heat treated specimens that had higher transverse properties and lower axial properties show more matrix/fiber adhesion. Specimens with the highest axial strength were weakest in the transverse direction. This indicates that the precipitation density was

too high. Higher temperature overaging would serve to reduce the precipitation density on interfaces.

5.2. Al-Cu-Mg and Al-Mg matrix composites

The influence of Mg on the properties of Al-based matrix composites is of great interest.

As demonstrated in Figure 5.3 the addition of 1.5% of Mg to Al-Cu matrix substantially reduced the axial properties, presumably because Mg attacked the alumina fiber during liquid melt infiltration. Note that as the time or temperature of the subsequent heat treatment increases, the strength of the composite decreases, leading to the conclusion that reaction continues in the solid state. Transverse properties as a result of fiber reaction with Mg are high. The fractography of transverse specimens (Figure 5.4) reveals numerous split fibers and strong matrix adhesion.

The Al-9.1%Mg composite, however, demonstrates high axial strength and moderate to low transverse strength as shown in Figure 5.5. The fracture surface of the transverse specimens shown in Figure 5.6 exhibits almost no fiber splits and rather clean fiber surfaces which have debonded from matrix. This trend does not agree with supposed reaction between Mg addition and alumina fiber. This behavior is explained by reaction passivation of the interface with increasing Mg concentration in the melt. Indeed, just recently it was shown by Lloyd and co-workers[7] that as the Mg concentration in the Al-based molten alloy exceeds about 5%, the thickness of the reaction product layer found on alumina particles surrounded by that melt was drastically reduced.

An interesting observation from the mechanical properties study is that in spite of copeous precipitation (see section 4.2.1) at the interface, heat treatment of Al-9.1%Mg matrix composite does not have a pronounced effect on either axial or transverse strengths of the composite. This indicates that precipitation per-se does not guarantee a strength increase. The controlling factor is the work of adhesion between the precipitate and fiber as compared to the work of adhesion between the precipitate and the matrix. For operation of the DCS principle, the work of adhesion between the precipitate and fiber should be the lesser value. If the work of adhesions (or bond strengths) are roughly equivalent, there will be no incentive for early debonding of the precipitates from the fiber and activation of interface delamination mechanism for interfacial toughening.

5.3. Al-Cu-Si-(Fe) and Al-Mg-Zn-(Fe) matrix composites

We will discuss and compare the mechanical properties of these composites in the same section of the report because they were both contaminated with iron during processing (see section 3.3) which reduced overall strength of these composites. Although useful information can be extracted if we compare the results for Al-Cu-Si and Al-Mg-Zn matrix composites, the Al-Si matrix composite was too

---

[7] D.J. Lloyd et al., " Controlling the interface reaction in alumina reinforced aluminum composites" , Scripta Met. v. 31 (94) pp. 393-396.)

contaminated to yield useful information and will be left for re-evaluation in Phase II.

The trends in axial and transverse strength for these two composites run in opposite directions as shown in Figure 5.7. In axial direction the Al-Mg-Zn matrix composite is much stronger than the Al-Cu-Si composite. This situation is reversed in the transverse direction where the Al-Mg-Zn matrix composite is very weak. The Al-Cu-Si composite shows one of the highest transverse strengths reported in this study. Fractography gives us the necessary insight to understand this phenomena.

Figure 5.8 shows the fracture surface of the transverse Al-Mg-Zn matrix composite. As we may see from the low magnification photo (a), the fiber surface and the matrix surface in the path of fracture appears to be very smooth. This suggests a weak fiber-matrix adhesion. Indeed, if we examine the surface of the matrix from which the fiber was pulled away (b), we see that it is densely covered with precipitates; hence, weak fiber adhesion to the precipitates at the fiber/matrix interface. In this particular case the precipitation density was excessive and the transverse properties were extremely low. Considering the degradation due to Fe contamination, the axial strengths were relatively high, .

For the Al-Cu-Si matrix alloy in Figure 5.9, we see the opposite picture. At low magnification, numerous fiber splits are evident. Traces of heavy plastic deformation of the matrix are noted. Bare fibers or smooth matrix surfaces are not present. At higher magnification, we see dimpled and heavily deformed matrix with a particle in the center of each dimple. These particles initiated the plastic fracture of the interface. In backscattered signal we can see that some of that particles contain Cu, but some of them do not. As expected, alloying with Si produced additional precipitates at the interface; however, Si addition apparently increased adhesion of the aluminum matrix to the fiber. The added adhesion suppressed any positive effect of the interfacial precipitation on the axial properties of the composite. However, by controlling the Si additions, we may be able to control the interface strength. In addition, this alloy would be excellent for discontinuously reinforced composites where strong adhesion between the matrix and reinforcement is advantageous.

6. 0 The Proposed Ductile Interface Precipitation Enhanced Toughening Mechanism and Supporting Observations

6.1. Toughening in brittle matrix composites versus ductile matrix composites

Control of toughness of a composite through control of the properties of the fiber/matrix interface is now well appreciated in the field of composites. One of the central concepts[8,9] of how the properties of the interface might be exploited for the purpose of improving the toughness of the composite, especially one with a brittle matrix, is to use the interface as a mechanical "fuse" deflecting the oncoming

[8]1. A.G. Evans, *Materials Science and Engineering*, A107 (1989), pp. 227-239.
[9] J.A. Cornie, AS. Argon, V.. Guppy, *Materials Research Society Bulletin*, v.16, 1991, pp. 32-38.

crack and thus protecting the fiber, as depicted in Figure 6.1. The unbroken fibers bridge the crack. Composite toughness is increased due to fiber pull-out and friction effects after eventual fracture. This concept pre-supposes inherently weak interfaces, usually produced by deposition of a weak coating on the fiber surface. The side-effect of such weak interfaces is a very low transverse strength, not to mention the high cost of fiber coatings.

Metal matrix composites with uncoated fibers are usually characterized as systems with strong fiber/matrix interface. One of the extreme cases for such strong interface is the aluminum/alumina fiber composite. Cracks in such composites, loaded in the direction of the fibers are never deflected along the interface. Therefore, fiber pull-out cannot be the main mechanism increasing toughness for such systems and main source of energy dissipation during fracture is different. Indeed, it has been pointed out by Friler et al[10] that after fracture of the fiber a great deal of mechanical energy is irreversibly consumed by plastic deformation of the surrounding matrix. Unlike the case of the weak interface for the brittle matrix composite, the crack is bridged not by the fiber, but by the plastically deforming matrix ligaments as shown schematically in Figure 5.2.

A simple geometrical analysis of the specific rupture work (X) in the matrix ligaments by Friler et al. gives:

$$\mathbf{X} = (\mathbf{Y}/\sqrt{3})\ (1-\sqrt{\mathbf{f}})\ \mathbf{L_d}\ \mathbf{h}(\varepsilon_\mathbf{f})$$

where **Y** is the equivalent tensile flow stress of the matrix, **f**, the volume fraction of fibers, $\mathbf{L_d}$, the total interface debond length and $\mathbf{h}(\varepsilon_\mathbf{f})$ (≤ 1.0), a geometrical function of the local strain to fracture in the matrix ligament which for dimple rupture has a limit of (1.0). It is clear from the development that additional toughening would be introduced if the deforming matrix ligaments could debond from the broken fiber ends - ideally to the natural rupture length of a freely necking metal strip deforming in plain strain. The driving force behind debonding is the "Poisson" contraction effect for plastically stretching matrix ligaments.

6.2. Role of the interfacial precipitation in increasing toughness in ductile matrix composites

The most probable mechanism of interface debonding for composites with a ductile matrix is the nucleation and growth of cavities at the interface. This mechanism can be initiated and controlled by introduction of micron-size, rigid particles at the interface which are more strongly bonded to the matrix than to the fiber.

The process of precipitation and coarsening in solid solutions, well-known from physical metallurgy, provides us with a convenient technique to produce rigid intermetallic particles at the interface. From a kinetics study of interface particles in a composite with Al-4.5%Cu matrix, the size of the interface precipitates is found to be controlled by the time of coarsening. An optimum average size of sub-micron precipitates is readily achievable as shown in Figure 4.5.

---

[10] JAB. Friler, AS. Argon, and J.A. Cornie, *Materials Science and Engineering*, A162 (1993), pp. 143-152.

Tests on the transverse strength of alumina fiber-Al-4.5%Cu composites, after different heat treatment times, reveal that the transverse strength for the specimens aged for a short time is lower than those aged for longer times, as shown in Figure 5.1.

The above results indicate that size and distribution of the precipitates control the process of fracture of the fiber-matrix interface. SEM fractography of the specimens fractured in the transverse direction support this hypothesis. Figure 6.3 shows the fracture surface of the interface on the matrix side as the fiber was torn away. It is clear that the fracture process was initiated between the fiber and precipitate particles and then the cavities developed around these sites. This is essential to preserve the intrinsic toughness of the matrix which contains the same particles.

6.3. $CuAl_2$: the right type of precipitate to trigger fiber debonding

Al-Cu matrix composites rely on $CuAl_2$ precipitates to trigger matrix debonding from the fiber. To be able to trigger fiber debonding, work of adhesion of precipitates to alumina should be lower than to the surrounding aluminum matrix. We have conducted a special experiment to verify this. In this experiment, using the pressure infiltration technique, a thin layer of aluminum alloy was put on top of the single crystal alumina plate. After that the composite was subjected to T7 treatment and then annealed at 400C for 150 hours. The resultant interface structure is shown in Figure 6.4. The contact angle for the precipitates on the substrate was then measured as shown in Figure 6.5. The resulting distribution is presented in Figure 6.6. From these data the work of adhesion of $CuAl_2$ to alumina was estimated. To compare the result with available literature data we also estimated the work of adhesion of $CuAl_2$ to alumina using the data of Eustaphopulos[11] and co-workers. To obtain this figure we have taken the data for pure Al and Cu on alumina substrate at high temperature and temperature dependence data for both elements. We extrapolated data for pure metals to 400C and then applied rule of mixtures. We can also obtain the value of the work of adhesion of $CuAl_2$ to aluminum using the data of L.C. Brown[12]. For easy comparison the data are presented in Table 6.1.

Table 6.1. Data on work of adhesion of $CuAl_2$ to alumina and aluminum from the literature and present study

Source Wad of $CuAl_2$ to....	Present Study	Data of Ref. 10	Data of Ref.11
Alumina	0.19-0.43 J/sq.m.	0.48 J/sq.m.	N/A
Aluminum	N/A	N/A	0.51-1.11 J/sq.m.

11 JAG. Li, Coudurier, L., Eustaphopolus, N., J. Materials Sci., 24, (1989), 1109-1116.

12 L.C. Brown. "Direct observations of coarsening in Al-Cu alloys" , Acta Met., 33, (1985),1391-1398.

The conclusion from the results presented in Table 6.1 is that $CuAl_2$ adheres stronger to aluminum matrix then to alumina fiber and is capable of initiating interface delamination.

6.4. Observations supporting the proposed model of fracture of the composite with ductile matrix and weakly adhered interfacial precipitates

If our model is correct we should be able to observe fractures similar to that depicted in Figure 6.2, in the fracture of a real composite. To make such an observation we have sectioned and polished fractured specimens parallel to the tensile and fiber axis. We chose a T7 heat treated Al-224.2 matrix composite as an example of a the system with strong interface and a specimen exposed to 350C for 10 hr as a system with a weak fiber/matrix interface. As Figure 6.7 shows, the fracture surface of T7 heat treated specimen is plain with occasional steps, which suggests brittle fracture and very little energy dissipation by deforming matrix. By contrast, Figure 5.8 shows a highly irregular fracture surface as seen at low magnification (a) and also at high magnification (b,c). The plastically deformed matrix ligaments have debonded from the fiber. An even closer look at the region of debonding (d) reveals the precipitates, which probably initiated interface decohesion, stuck to the matrix side of the fracture surface. These observations correspond well to the proposed model and provide insight into how the composite with weak interface and ductile matrix fractures. With this "smoking gun" in hand, we finally have the tools to design matrices for continuously reinforced composites.

7.0 Conclusions and Discussion

1. Several aluminum based alloys capable of producing the discontinuously coated interface effect were tried as a matrix material for alumina fiber - aluminum composites.

The addition of 1.5% Mg to Al-4.5%Cu matrix alloy drastically reduced the axial strength of composite, but strongly increased the transverse strength. The strength reduction continued with increasing thermal exposure time. The reaction of Mg with alumina fiber is the proposed reason for such behavior.

However, the Al-9.1% Mg alloy did not degrade the fiber strength. The increase of Mg concentration causes a passivation effect on the reaction layer at the interface. Though the precipitation at the interface induced by heat treatment was very dense, the mechanical properties showed no response. This indicates the fundamental importance of the work of adhesion between given type of precipitate and the fiber. The work of adhesion between a precipitate and the fiber must be lower that between the precipitate and the matrix for the precipitate to play a role in interface delamination and the DCI effect to become operative. Low Mg alloys are unsuitable for systems continuously reinforced with alumina fibers. However, low Mg alloys would be ideal for systems discontinuously reinforced with alumina particulates.

The most promising results were shown by Al-9.5%Mg-5%Zn composites: The transverse strength fell dramatically as a result of super-active interfacial

precipitation. The fiber/matrix interface remained clean and smooth as shown by transverse specimen fractography. A lower Zn alloy would be a good choice for continued evaluation in Phase II.

Silicon alloying of the Al-4.5%Cu matrix produced extra precipitates at the fiber-matrix interface after heat treatment in addition to $CuAl_2$ particles. However, the transverse strength was very high for that alloy, and the axial strength was low. Presumably Si increased adhesion of aluminum to alumina. A lower Si alloy or modified heat treatments should be the action item for continued investigation into the Al-Cu-Si system in Phase II.

2. The kinetics of coarsening and precipitation process at the interface was studied for Al-Cu, Al-Mg and Al-Cu-Mg matrix composites. The size of precipitates increases as $t^{1/4}$. This result coincides with theoretical prediction. However, particle size distribution does not agree with theory for Al-Cu and Al-Cu-Mg matrix composites. For Al-Mg matrix composites the shape of particles size distribution is closer to theoretically predictions.

We can use the kinetics results us a tool to tailor interface structure and control interface properties. Judicious selection of alloy systems and the design of heat treatments will be the operational approach of the Phase II effort.

3. A new model for the toughening of the composite with a ductile matrix and weakly bonded precipitates at the interface is proposed. The experimental observations strongly support the proposed model.

4. A new highly productive technology for pressure infiltration of composites was tested in this study.

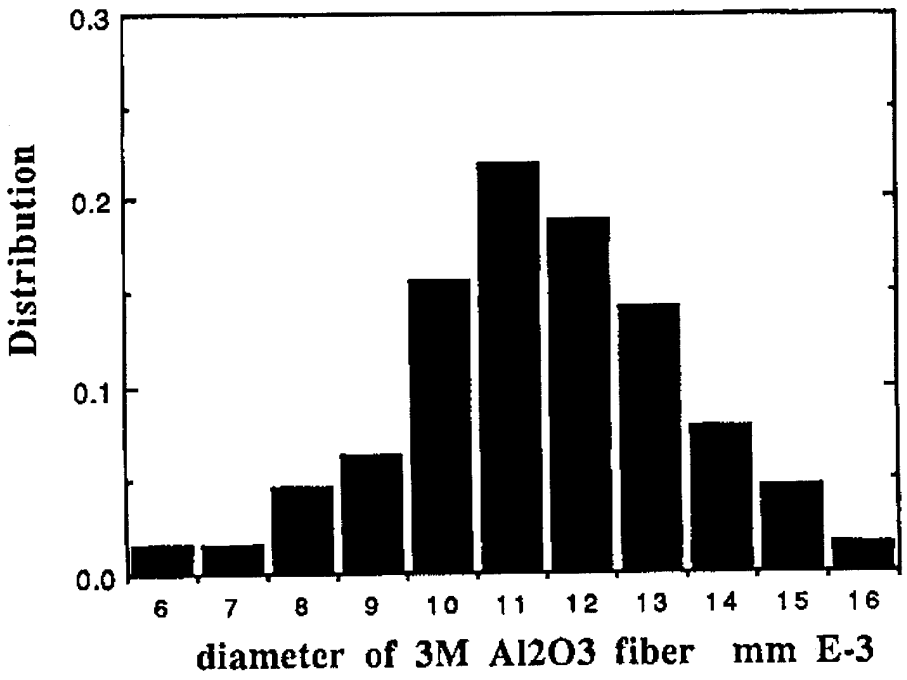

Figure 3.1 Example of 3M fiber size distribution.
Average Fiber Diameter = 11.5 μm

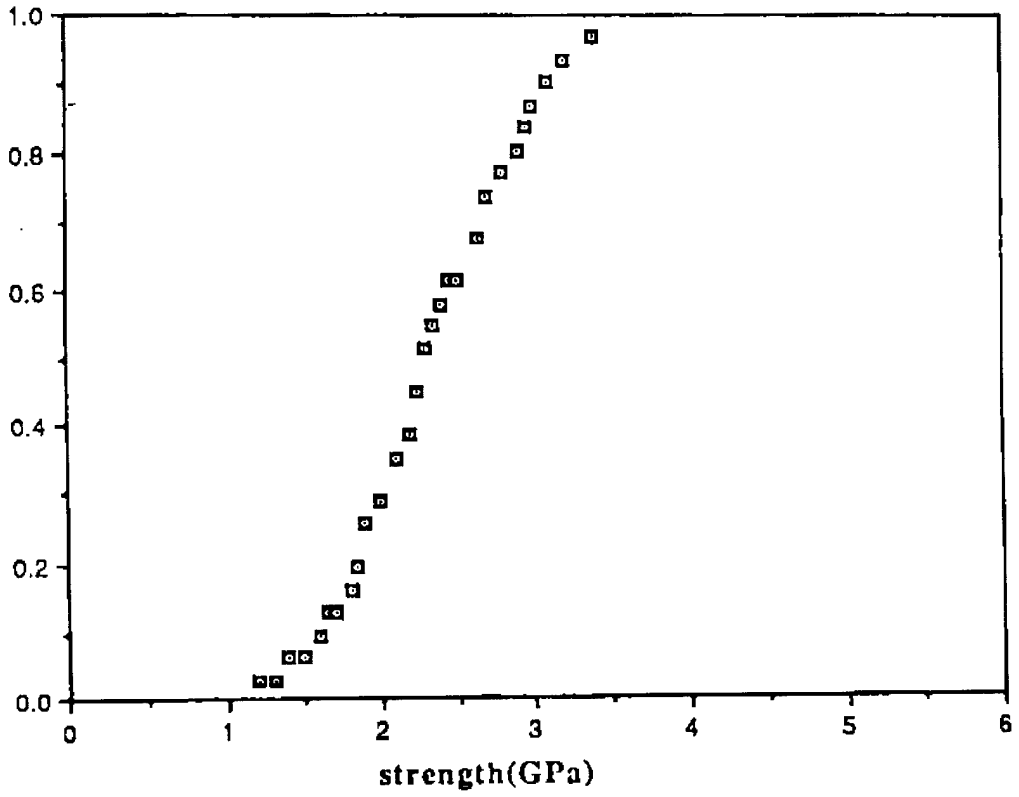

Figure 3.2 Example of cumulative fiber strength distribution for 3M Nextel 610 fiber.

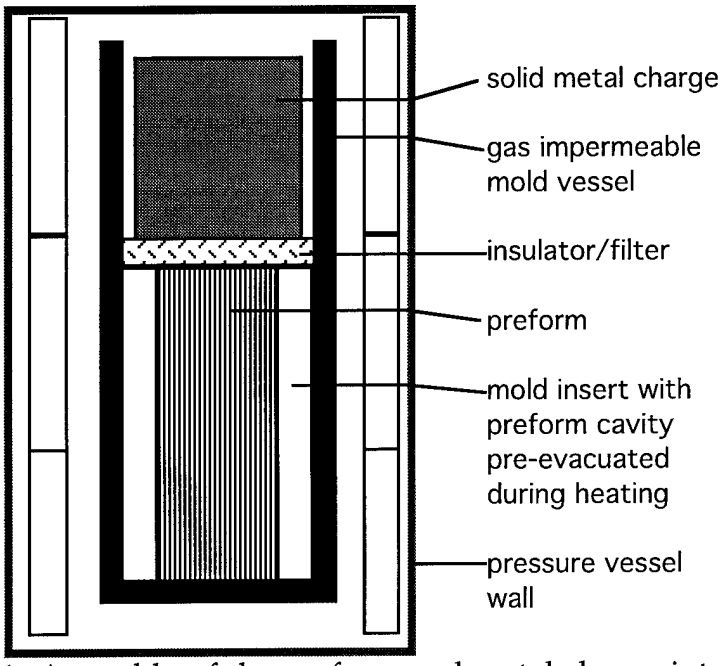

Figure 3.8-a. Step 1- Assembly of the preform and metal charge into mold vessel and insertion into the pressure vessel.

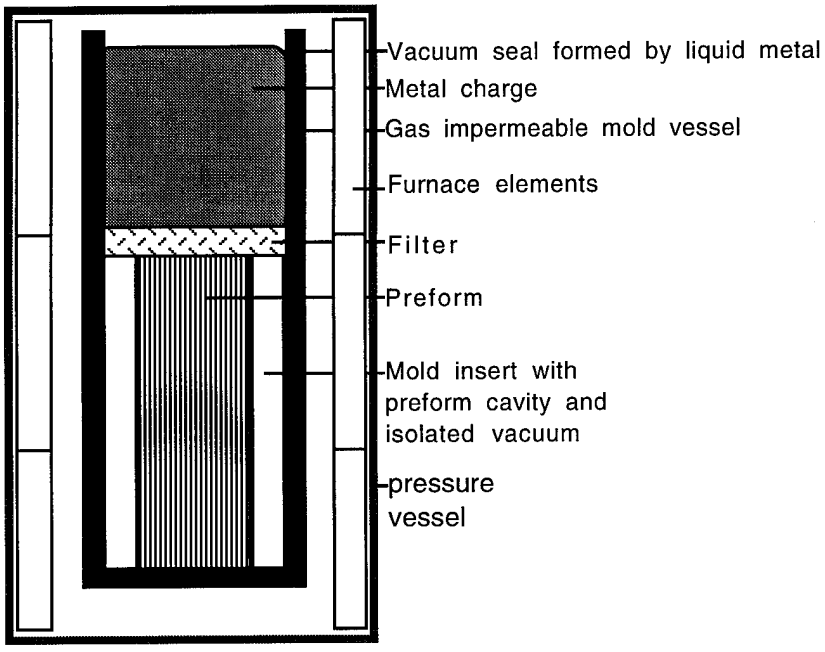

Figure 3.8-b Step 2-Isolating a vacuum in the mold cavity by the formation of a vacuum seal at the melt charge/mold vessel interface.

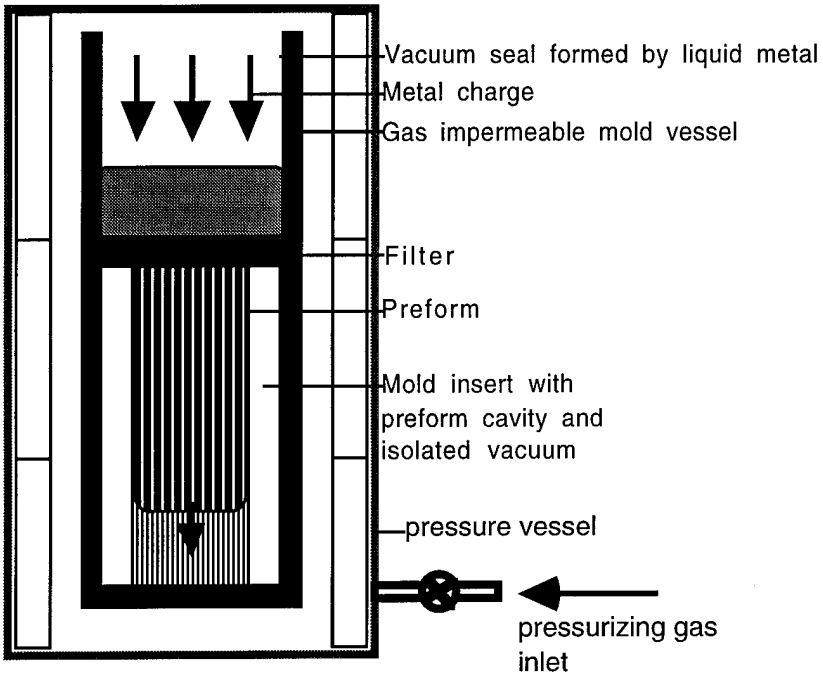

Figure 3.8-c Step 2-Isolating a vacuum in the mold cavity by the formation of a vacuum seal at the melt charge/mold vessel interface.

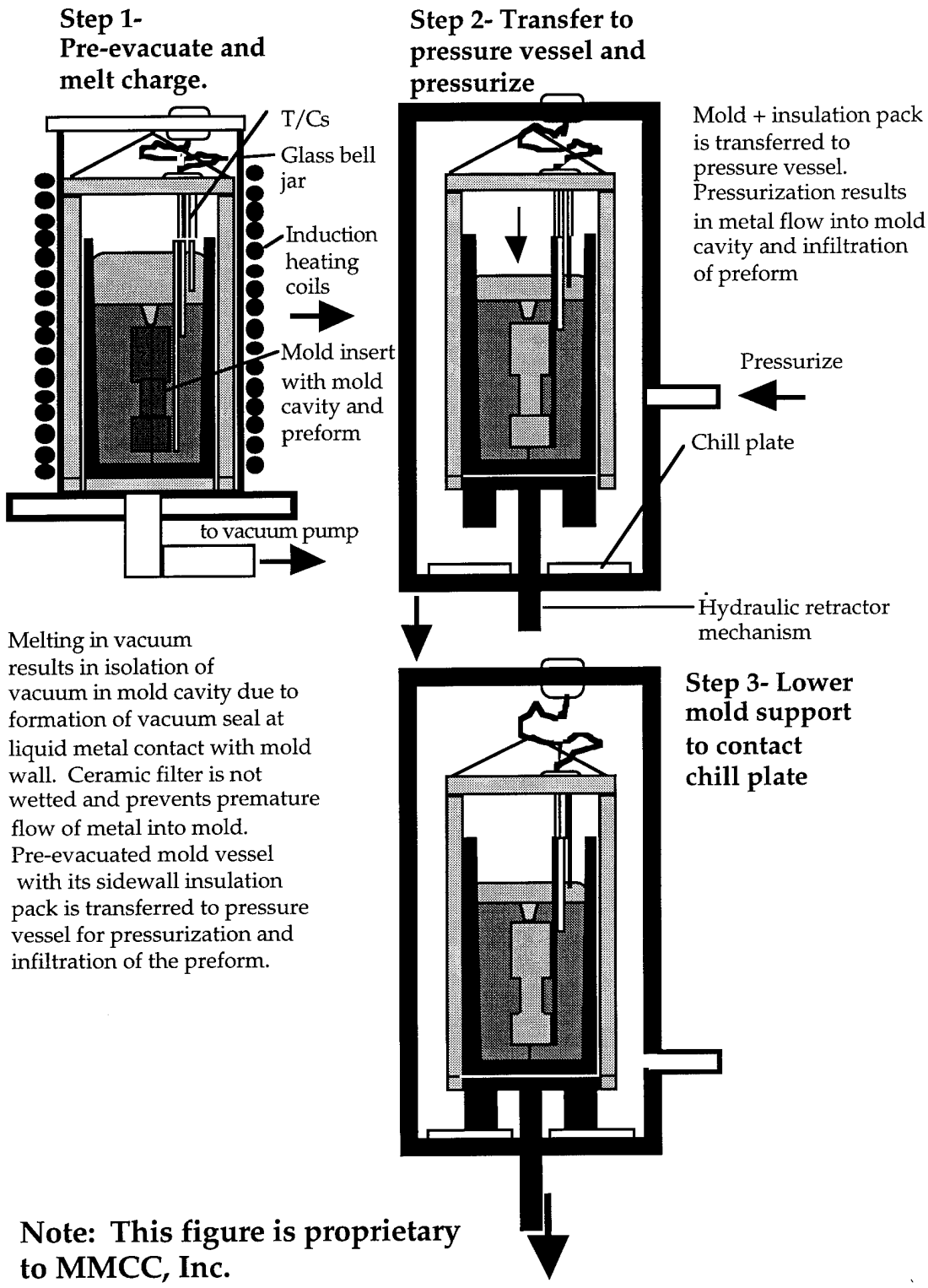

Figure 3.9 Schematic of the new technology developed at the MMCC.

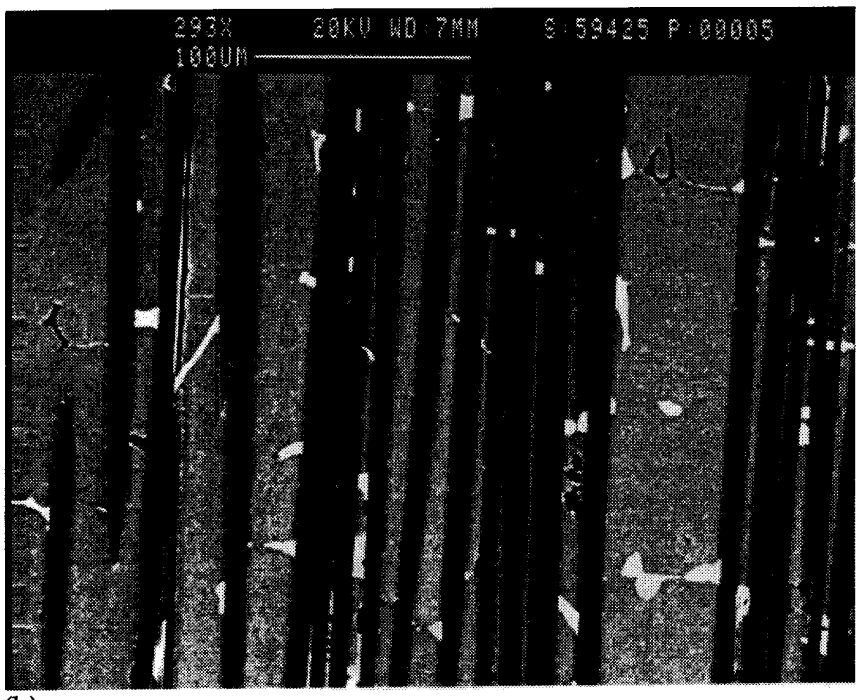
293X 30KV WD:7MM S:59425 P:00005
100UM

(b)

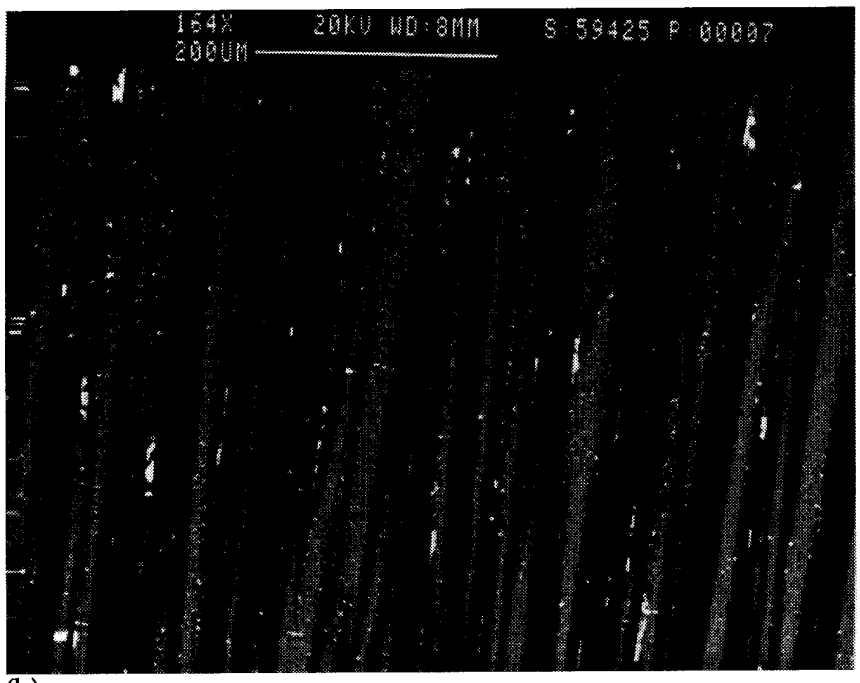
164X 20KV WD:8MM S:59425 P:00007
200UM

(b)

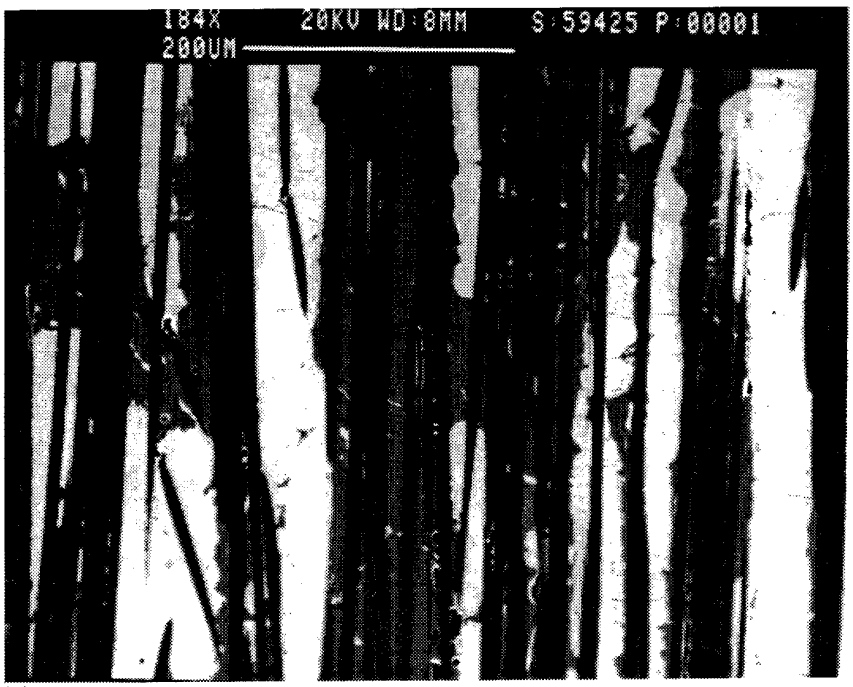

(c)

Figure 3.10 The iron-rich brittle phases (large bright particles) in the structure of iron-contaminated Al-9.5%Mg-1.5%Zn (a), Al-4.5%Cu-1.2%Si (b) and Al-4%Si (c) composites. (photo: 59425-5, 59425-7, 59425-1)

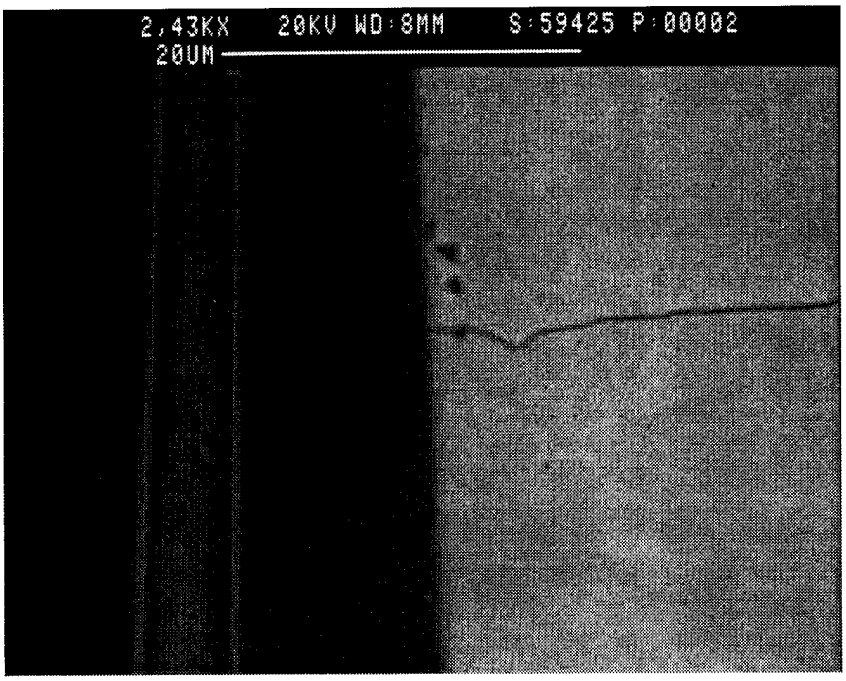

Figure 3.11 The crack initiated in iron-rich phase penetrates adjacent fiber. (photo 59425-2).

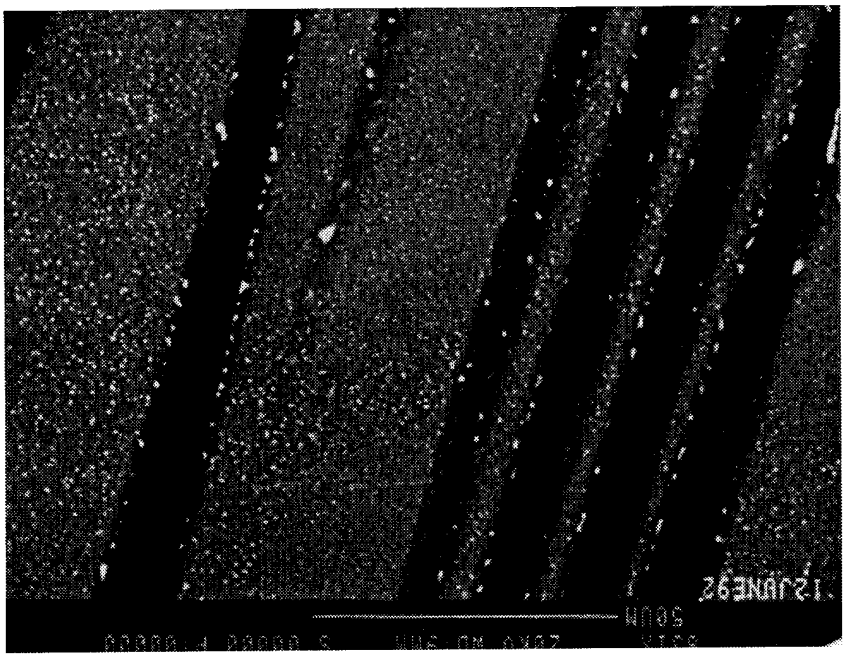

Figure 4.1. The enhanced precipitation at the fiber-matrix interface. Matrix: Al-224.2 Al alloy. Heat treatment: T7+10h at 350C.

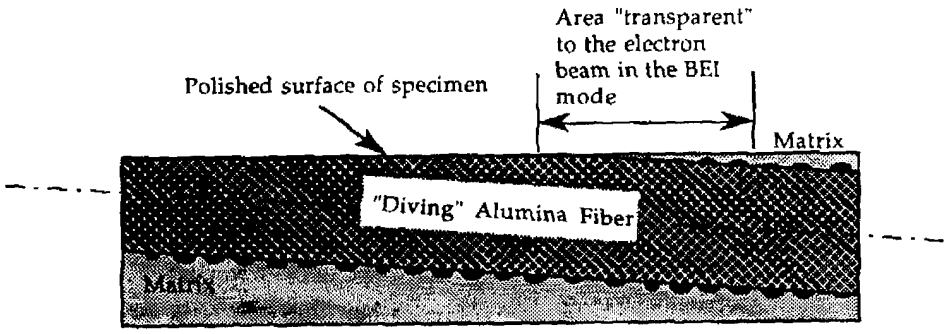

Figure 4.2. The schematic of the method to observe precipitates at the fiber-matrix interface using SEM backscattered electrons signal.

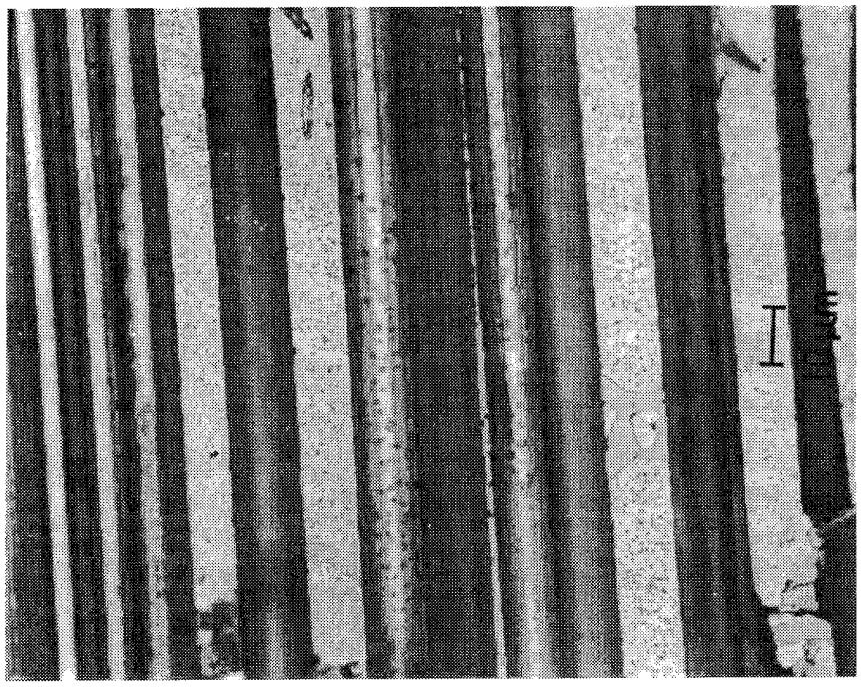

Figure 4.3 Interface precipitates as seen through transparent fiber body.

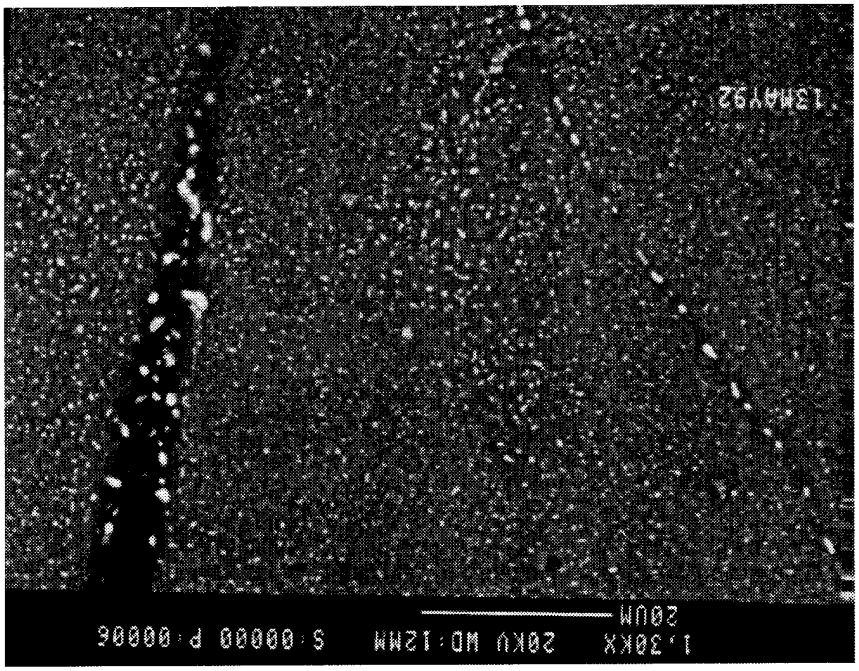

Figure 4.4 Enhanced precipitation of $CuAl_2$ at the fiber-matrix interface shown along with the enhanced precipitation of the same phase at the grain boundary. Matrix: 2.24 Al alloy. Heat treatment: T7+350C 10h.

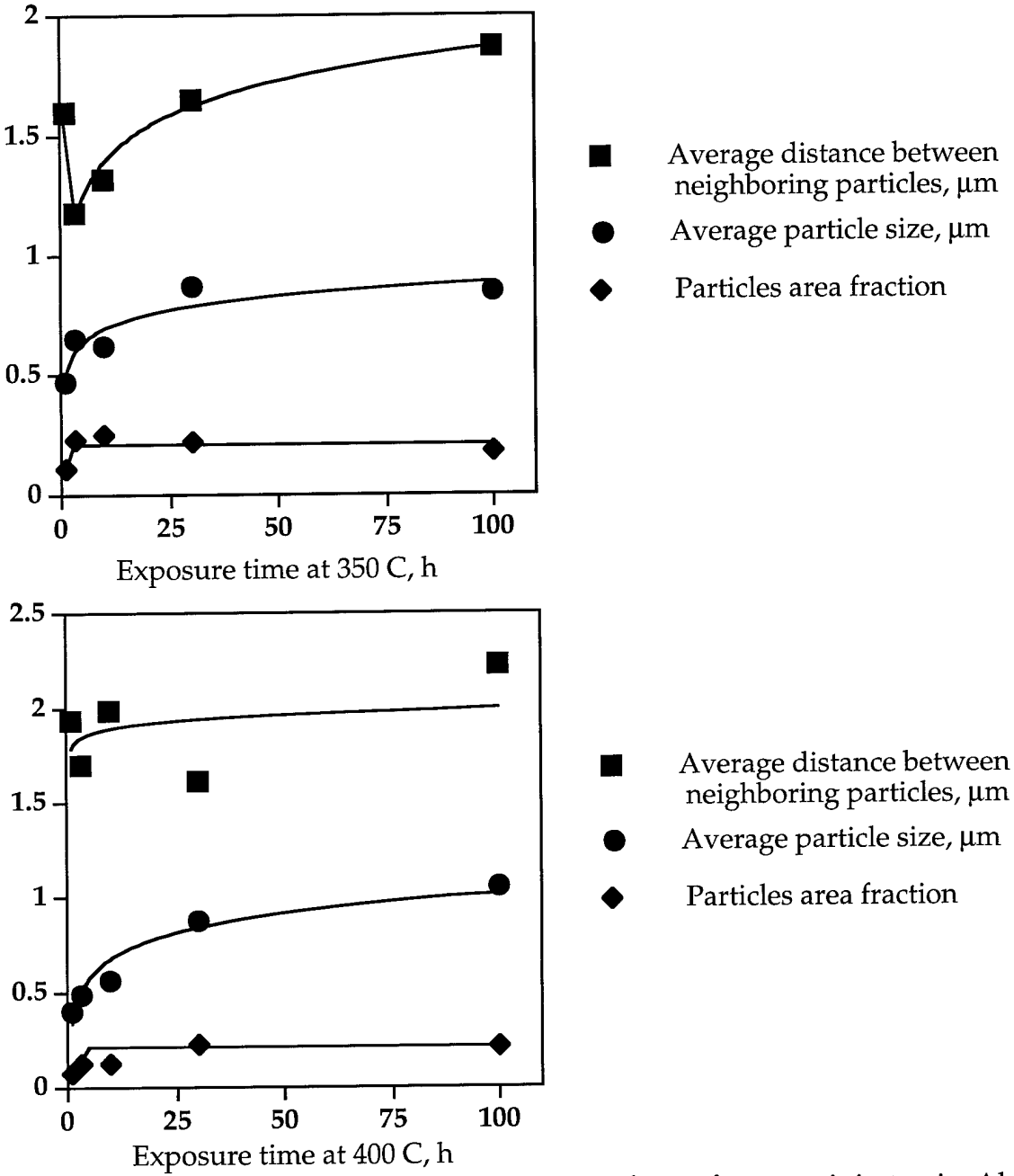

Figure 4.5. Microstructural characterization of interface precipitates in Al-4.5%Cu matrix composite after annealing at 350C and 400C.

Shape of coarsening particles size distribution : experiment vs. theory.

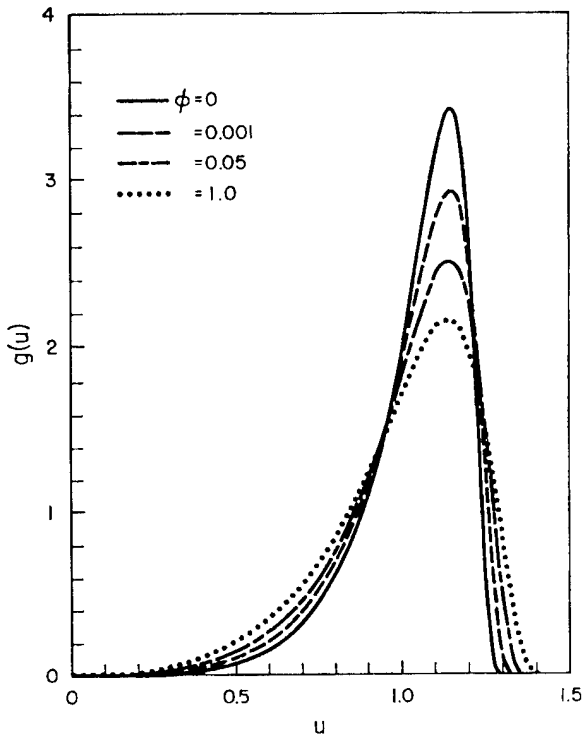

(a)

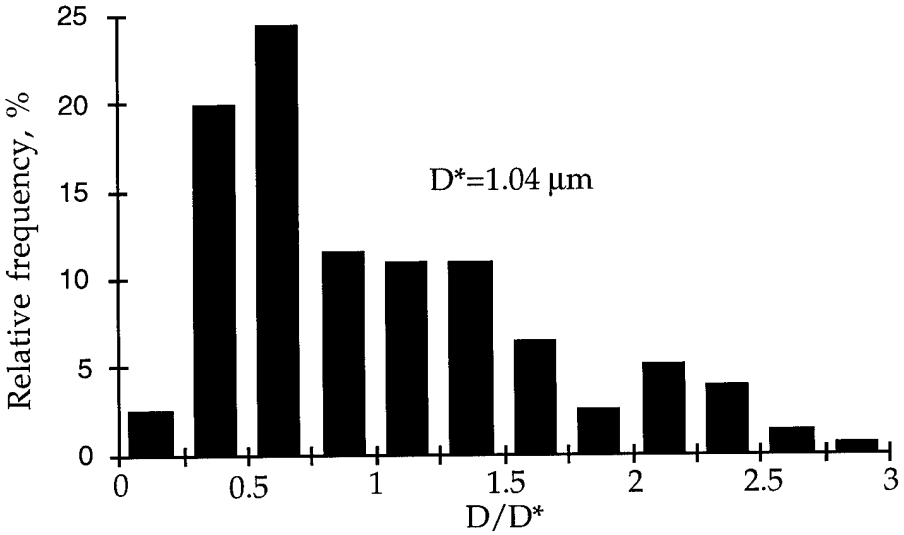

Distribution of precipitates sizes at the interface in Al-4.5%Cu matrix composite after annealing at 400C for 100 h.

(b)

Figure 4.6. Shape of theoretical size distribution function (a) and experimental particle size distribution (b)

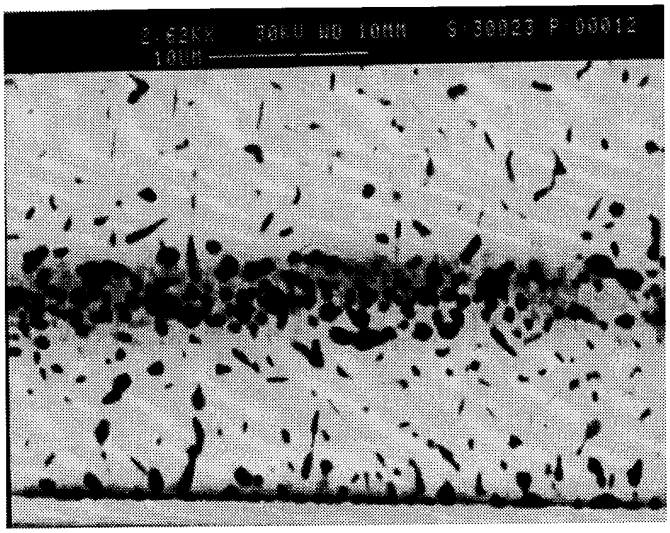

Figure 4.7 The interfacial precipitation in Al-9.1% Mg matrix composite after 23 hours at 300C.

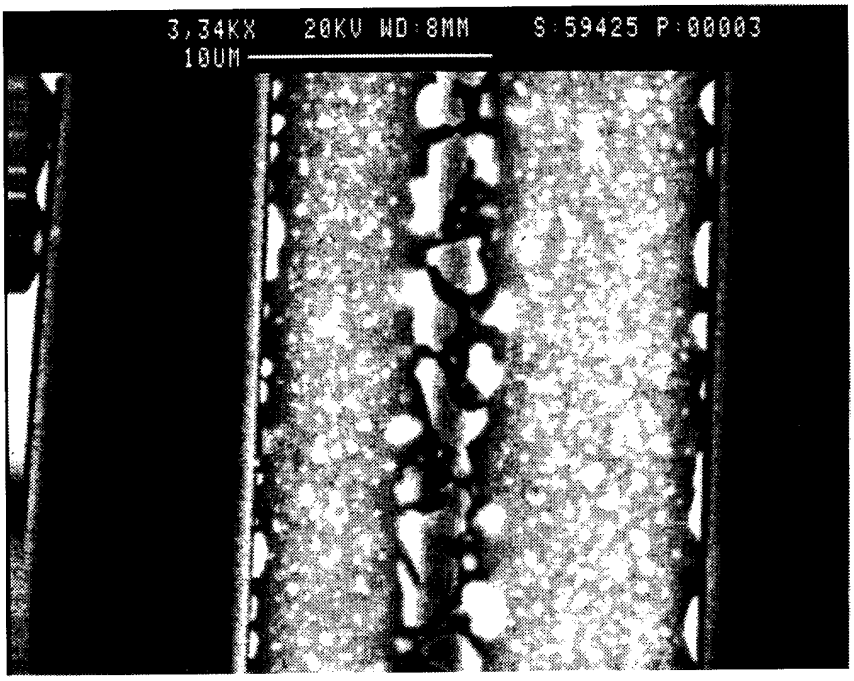

Figure 4.8 Precipitation at the fiber-matrix interface in Al-9.5%Mg-5%Zn matrix composite. Heat treatment: T7 + 48h at 300C.
(Photo 59425 03).

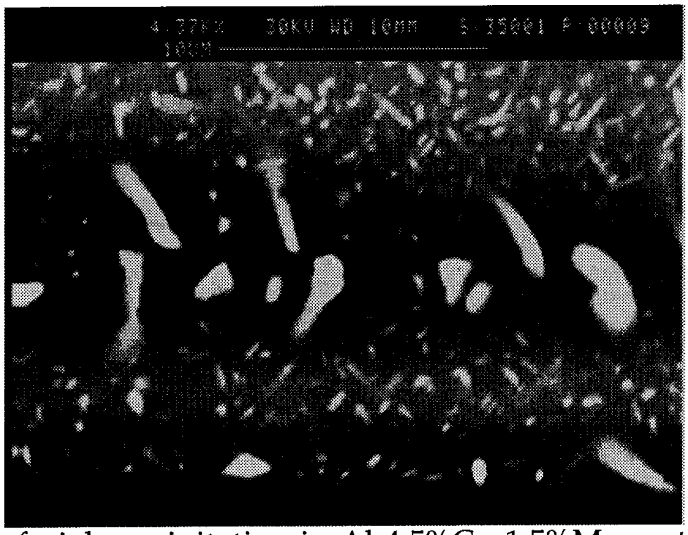

Figure 4.9 The interfacial precipitation in Al-4.5%Cu-1.5%Mg matrix composite after 30 hours at 350C.

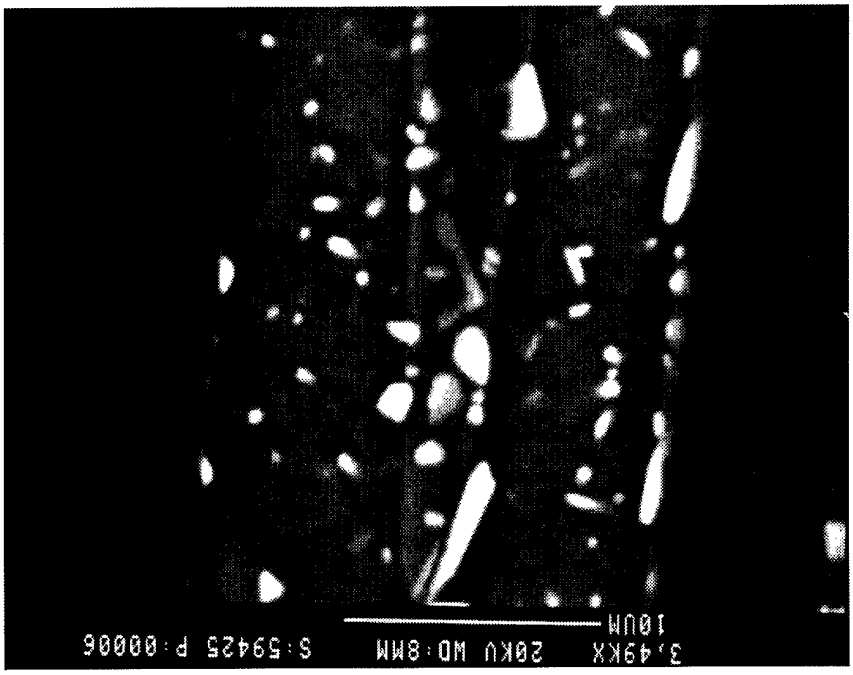

Figure 4.10 The interfacial precipitates in Al-4.5%Cu-1.2%Si composite. Heat treatment: T7+48h at 400C.
(Photo 59425-6)

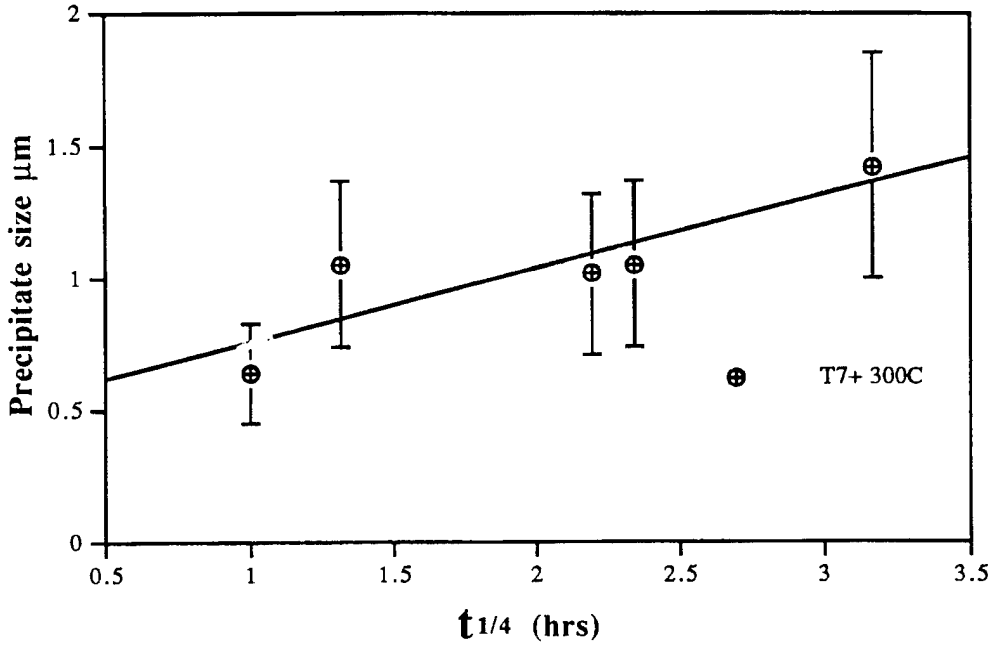

Figure 4.11 Interfacial precipitates size vs. time to 1/4 in Al-9.1% Mg composite.

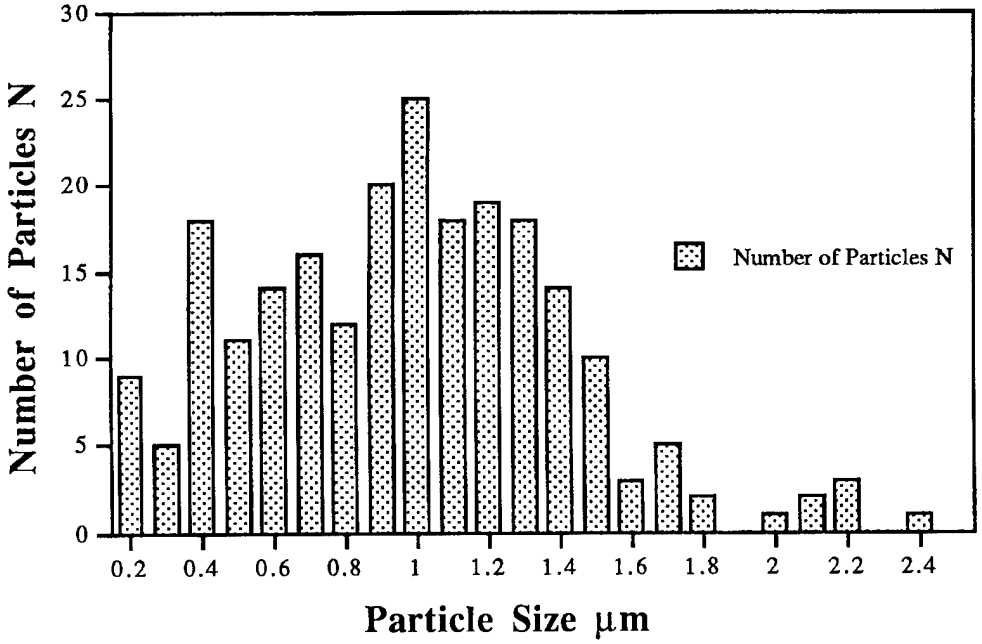

Figure 4.12 The interfacial particle size distribution during coarsening in Al-9.1%Mg matrix composite. Heat treatment: 3h at 300C.

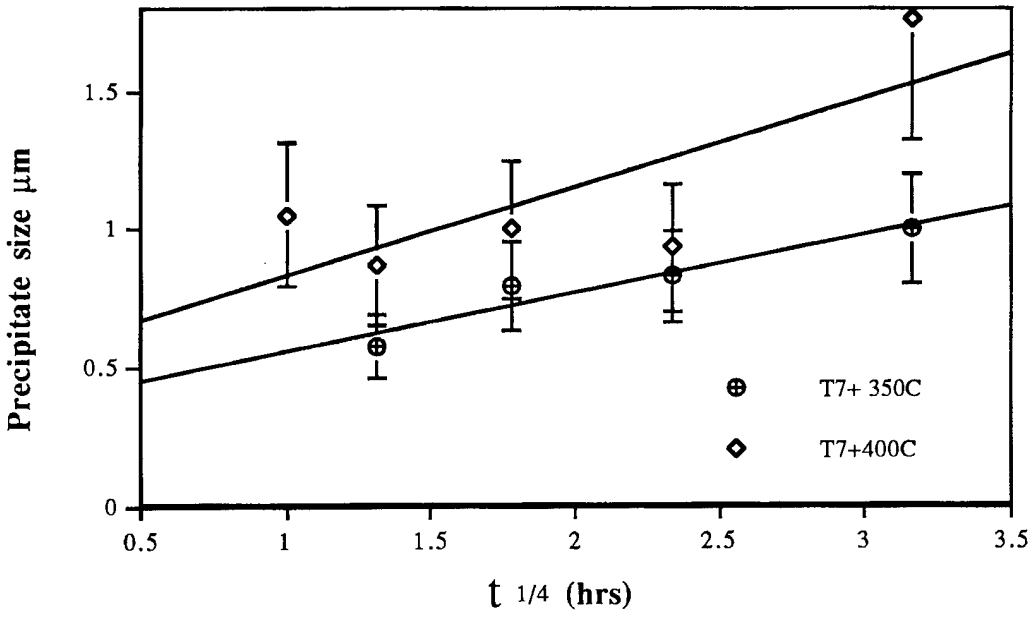

Figure 4.13 Interfacial precipitates size vs. time to 1/4 in Al-4.5%Cu-1.5% Mg composite.

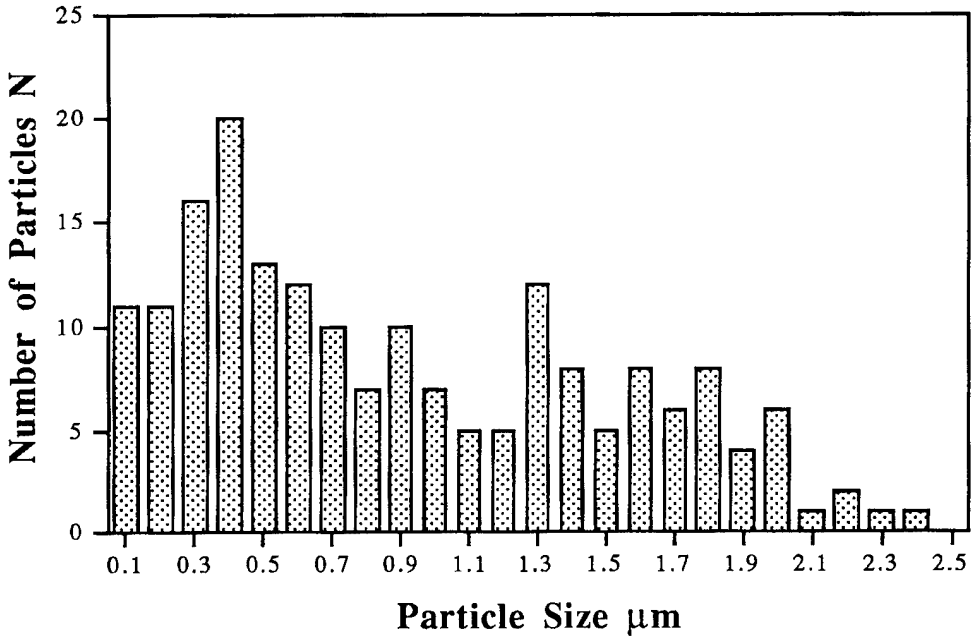

Figure 4.14 The interfacial particle size distribution during coarsening in Al-4.5%Cu-1.5%Mg matrix composite. Heat treatment: 100h at 350C.

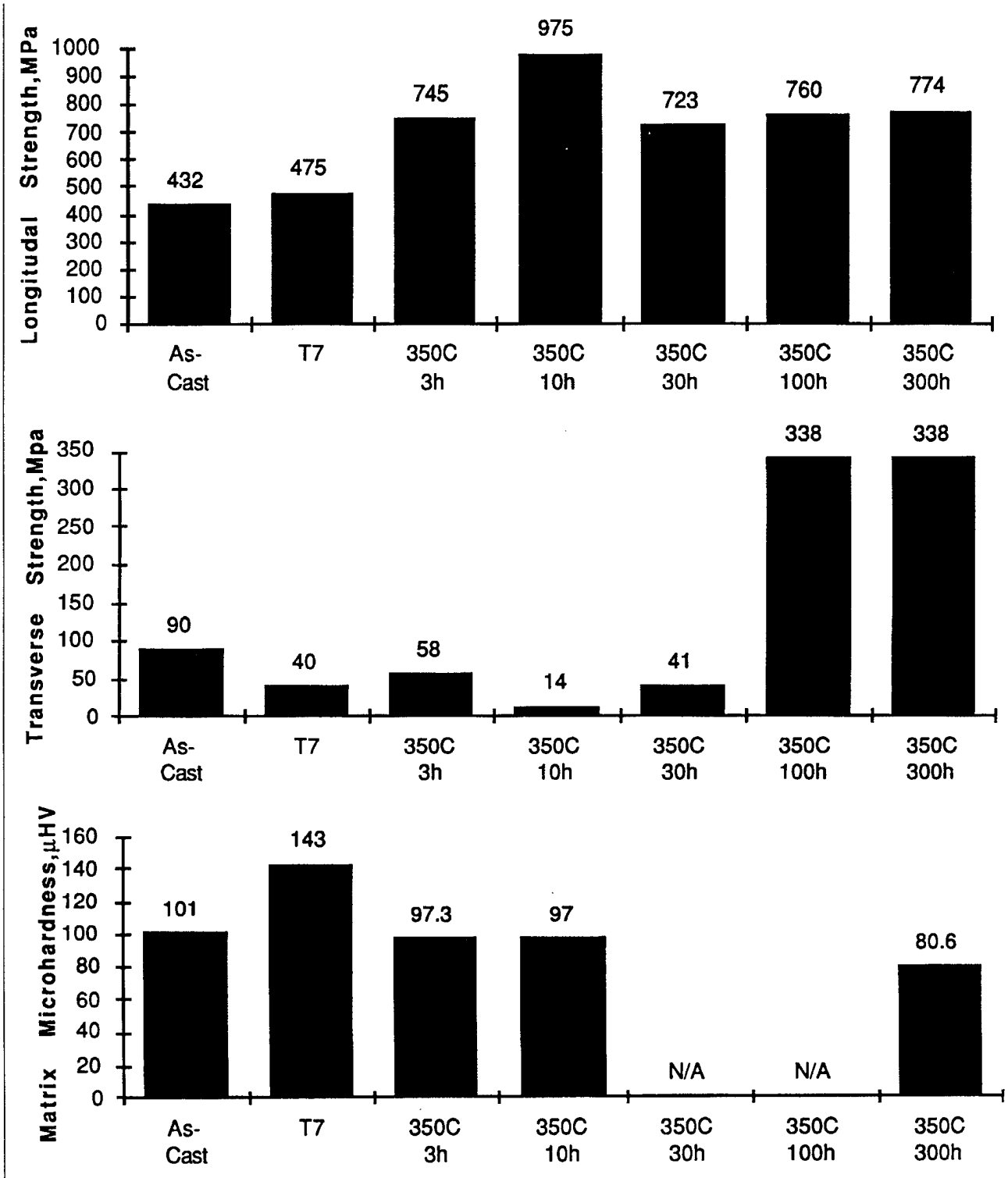

Figure 5.1 Longitudinal and transverse strength of alumina-224.2 Al alloy matrix composite after standard (As-Cast and T7) and 350C heat treatments. Also shown the microhardness of the matrix material after the same treatments.

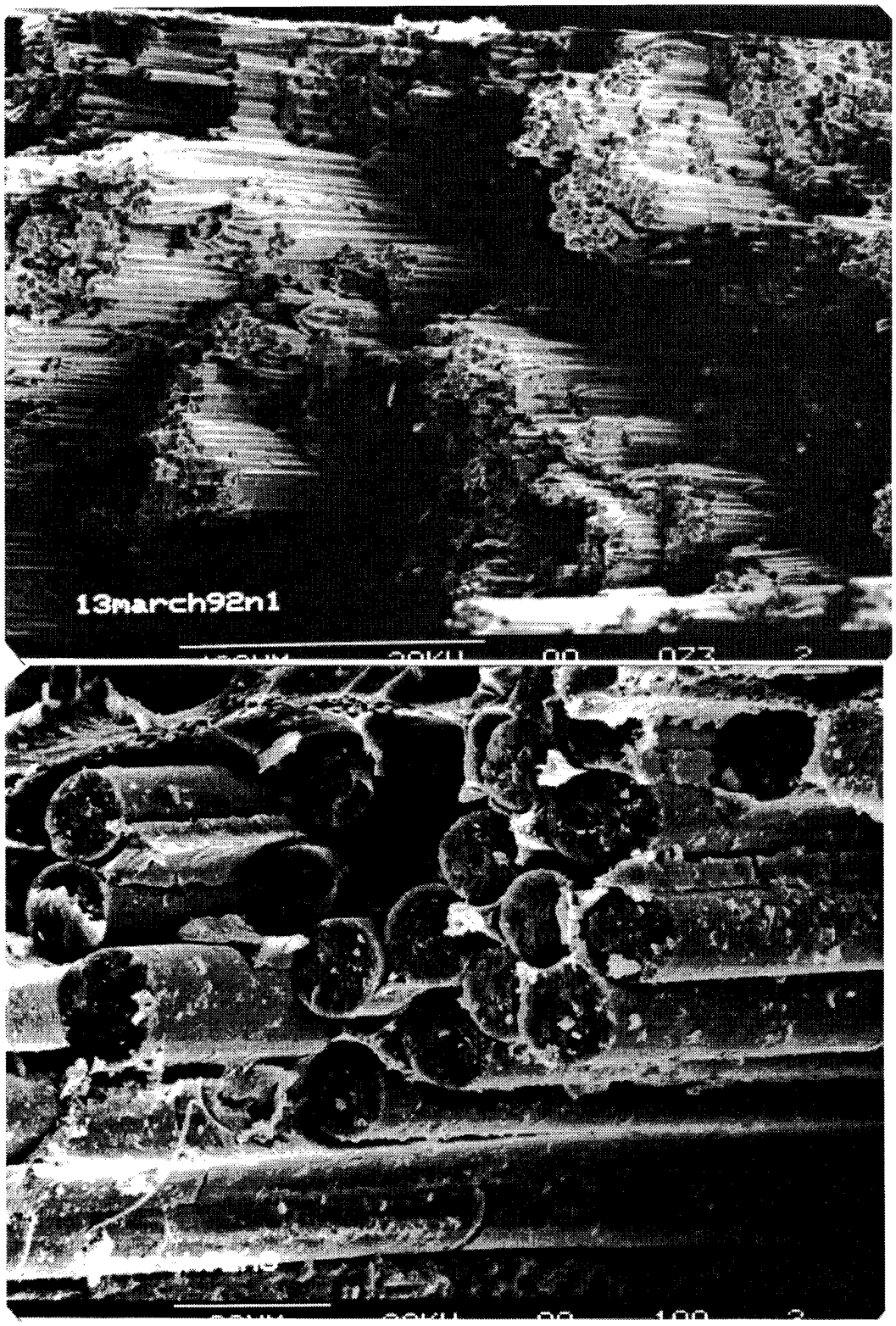

(a)

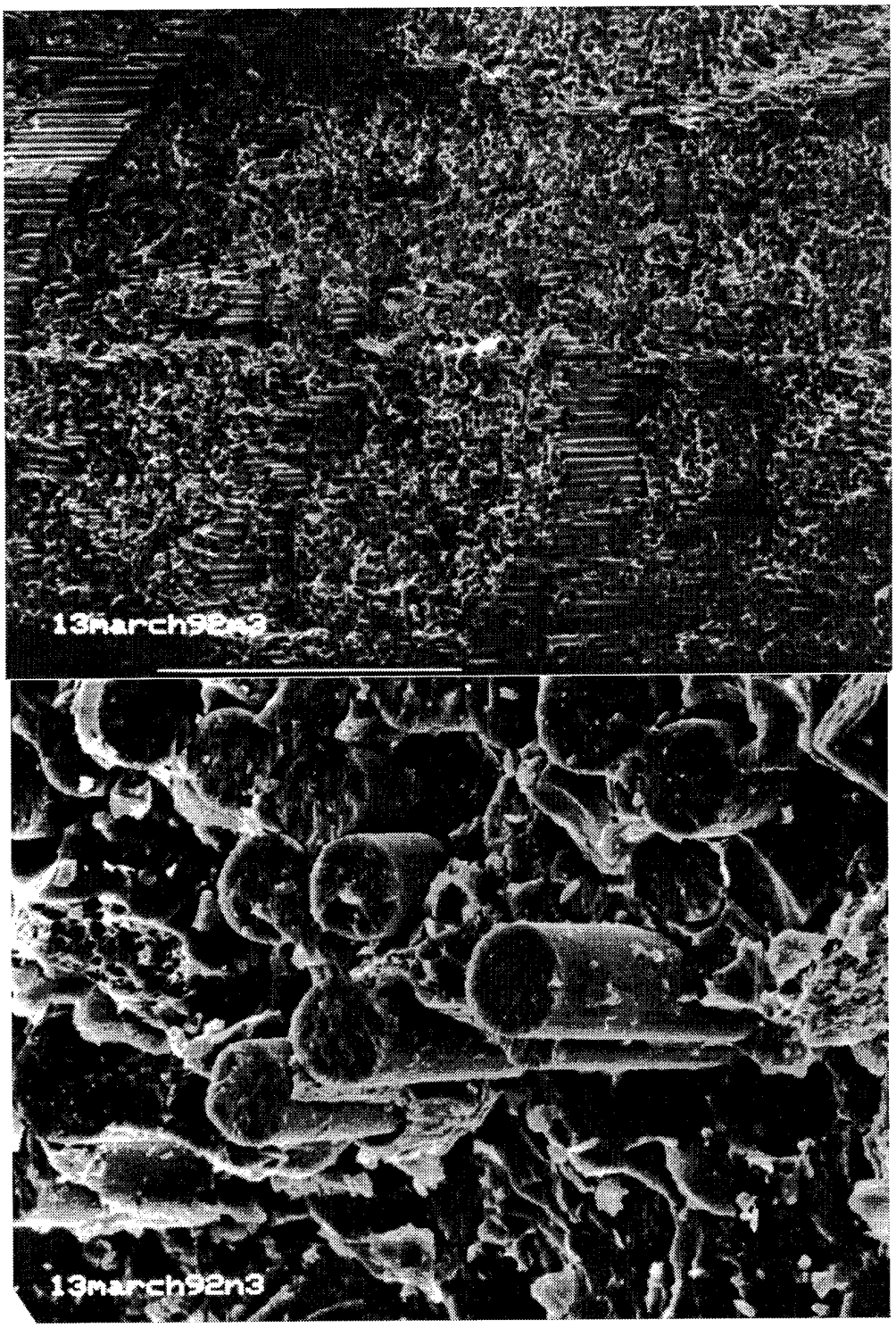

(b)

Figure 5.2 The fracture surface of the axial specimen exposed to 350C for 10h (a), as compared to T7 heat treated specimen (b).

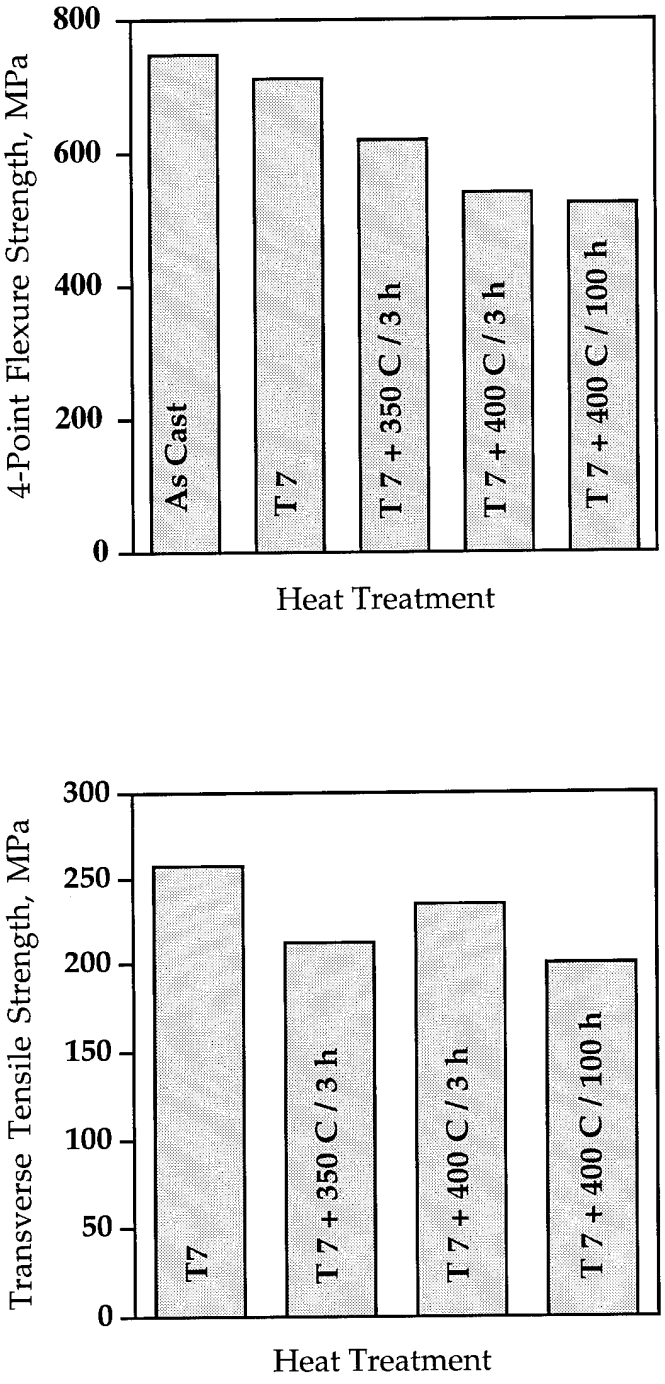

Figure 5.3 Mechanical properties of Al-4.5%Cu-1.5%Mg composite after heat treatments.

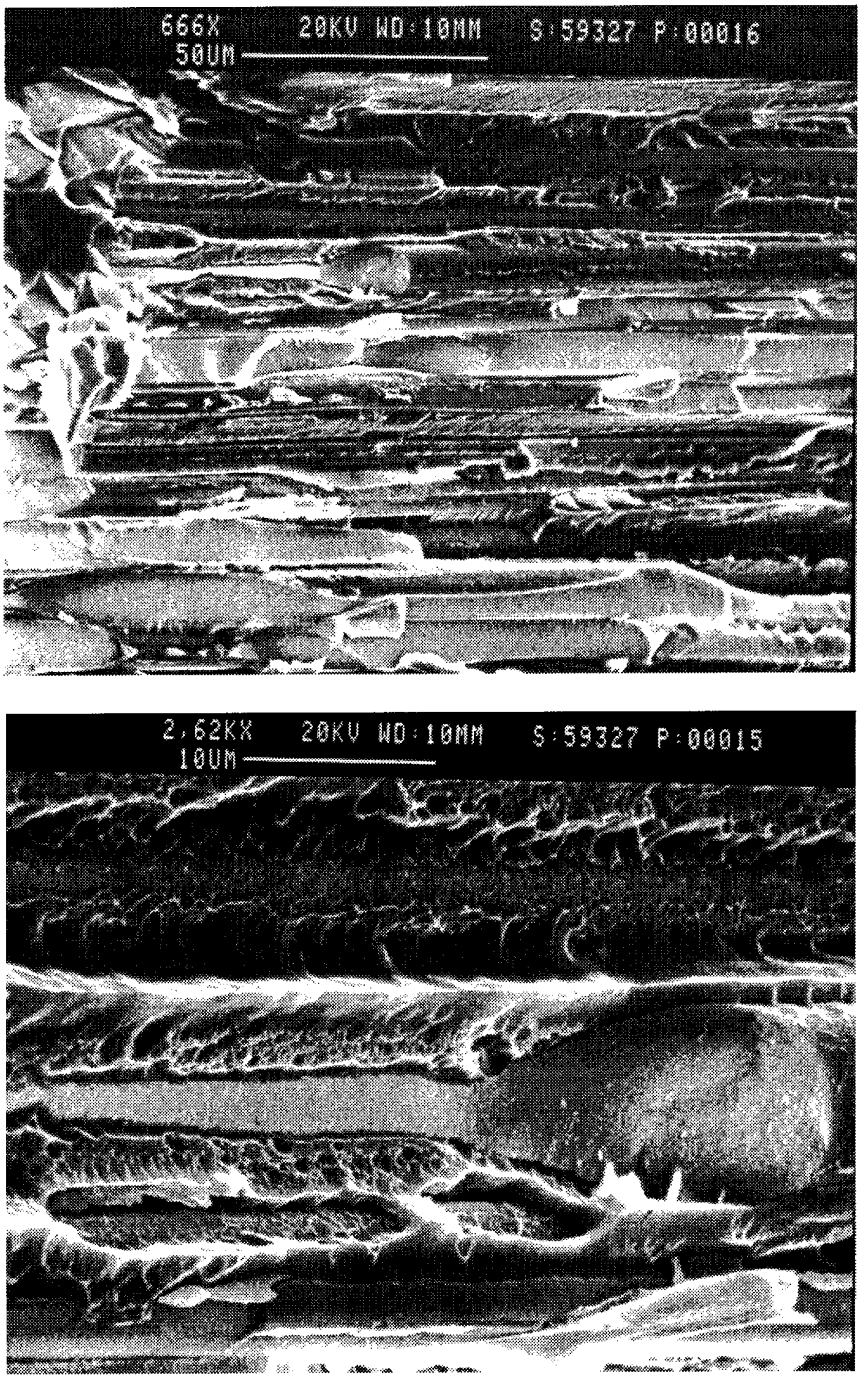

Figure 5.4 Fracture surface of the transverse Al-4.5%Cu-1.5%Mg matrix composite at low (a) and high (b) magnification.
(Photo 59327-16, 59327-13)

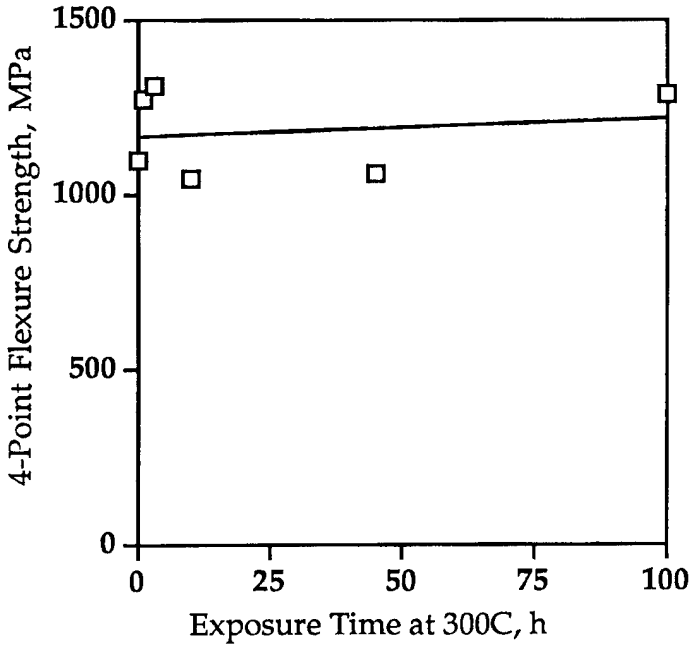

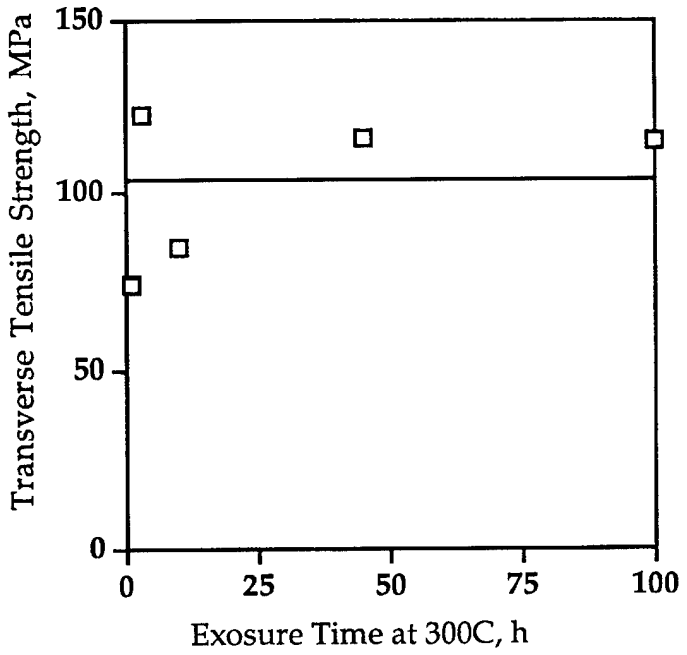

Figure 5.5 Mechanical properties of Al-9.1%Mg matrix composite after different heat treatments.

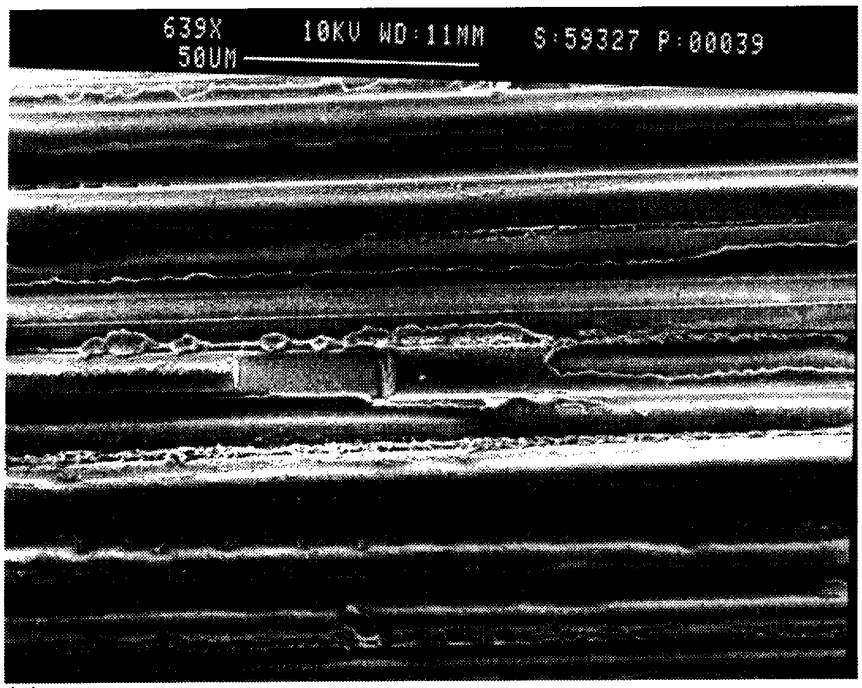

(a)

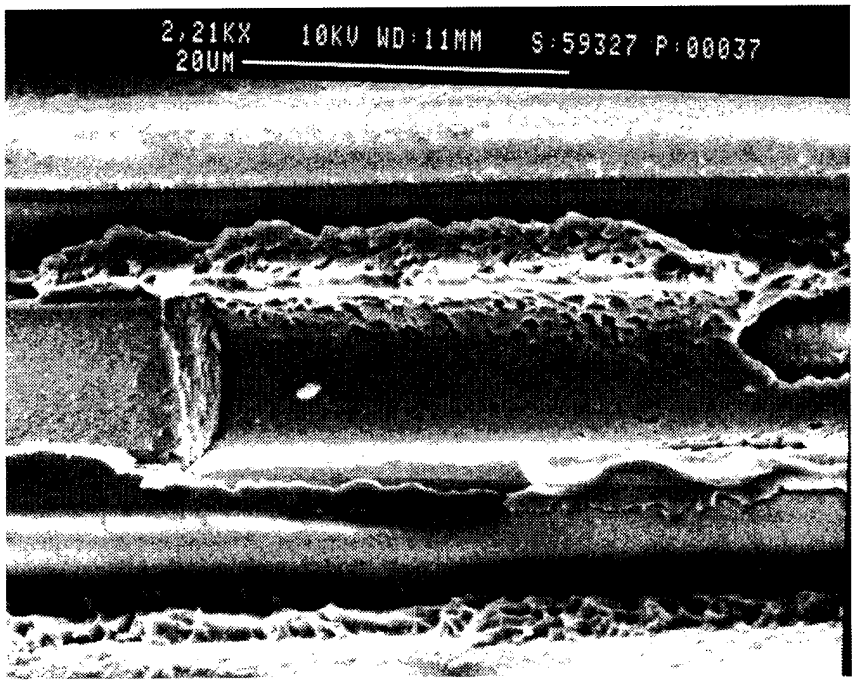

(b)

Figure 5.6 The fracture surface of the transverse Al-9.1%Mg matrix composite at low (a) and high (b) magnifications.
(Photo 59327-39, 59327-37).

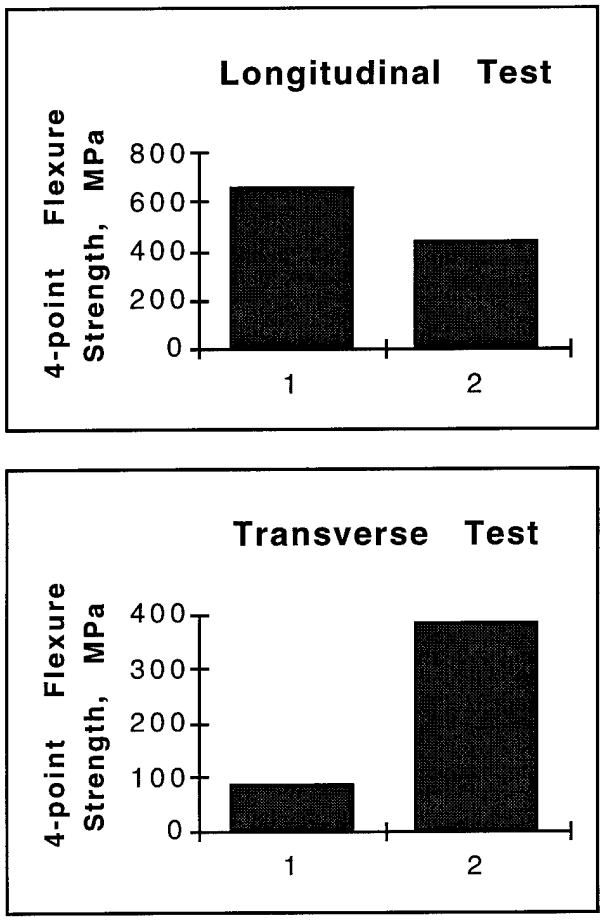

Figure 5.7 Comparison of longitudinal and transverse strength of Al-9.5%Mg-5%Zn (#1) and Al-4.5%Cu-1.2%Si (#2) composites.

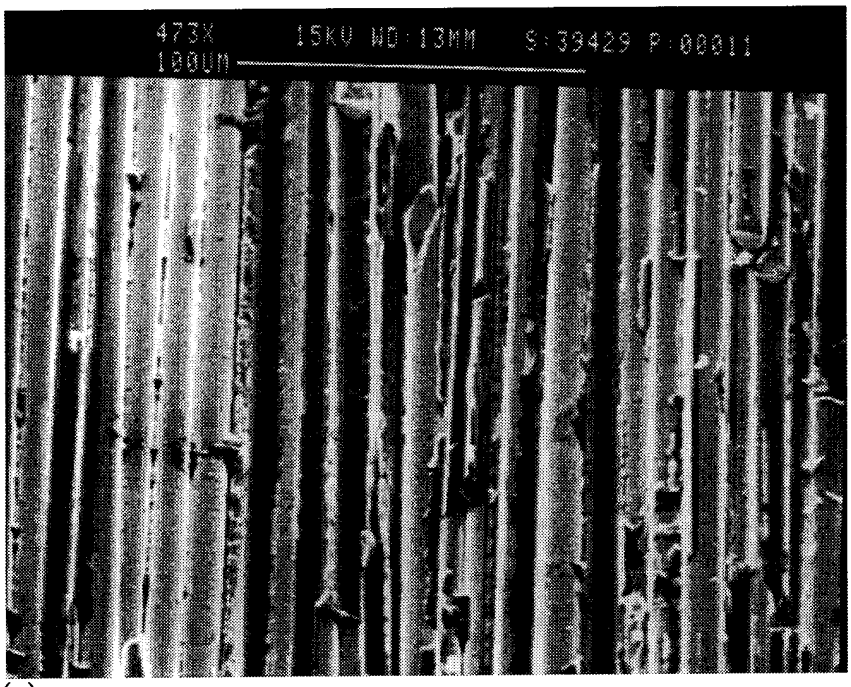

(a)

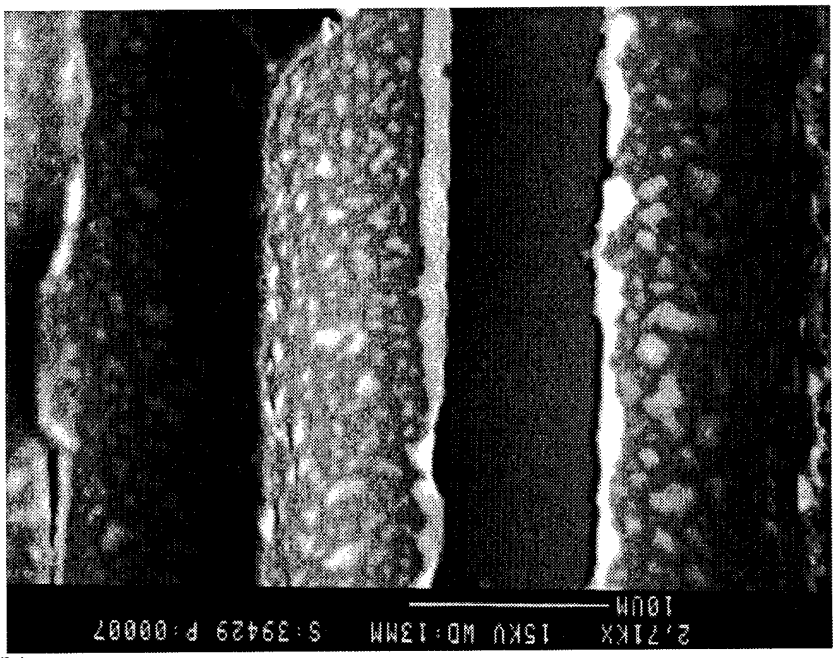

(b)

Figure 5.8 Fracture surface of Al-9.5%Mg-5%Zn composite at low magnification in secondary electrons contrast (a) and at high magnification in backscattered electrons contrast (b).
(Photo 39429-11, 39429-7)

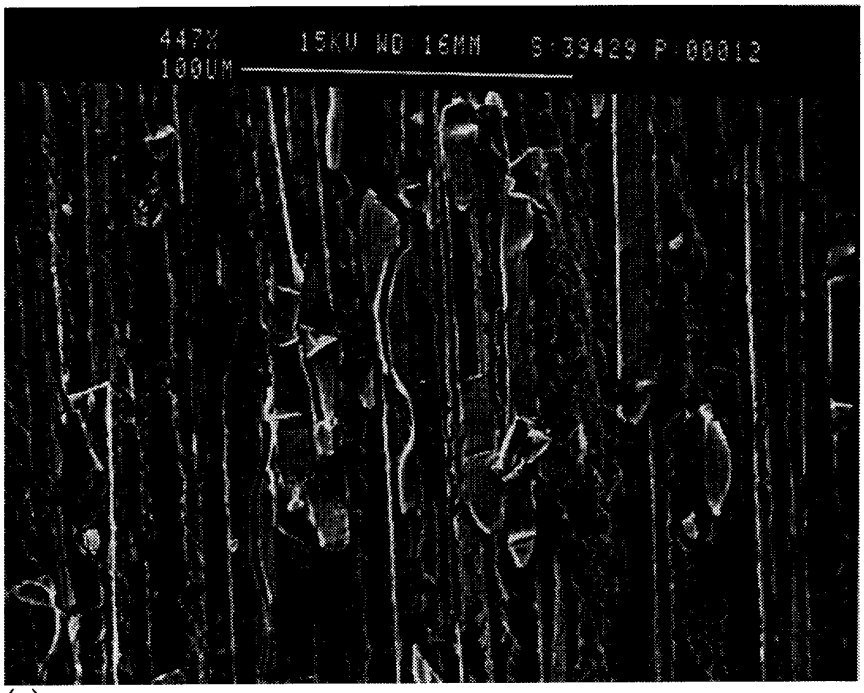
447X 15KV WD 16MM S-39429 P-00012
100UM

(a)

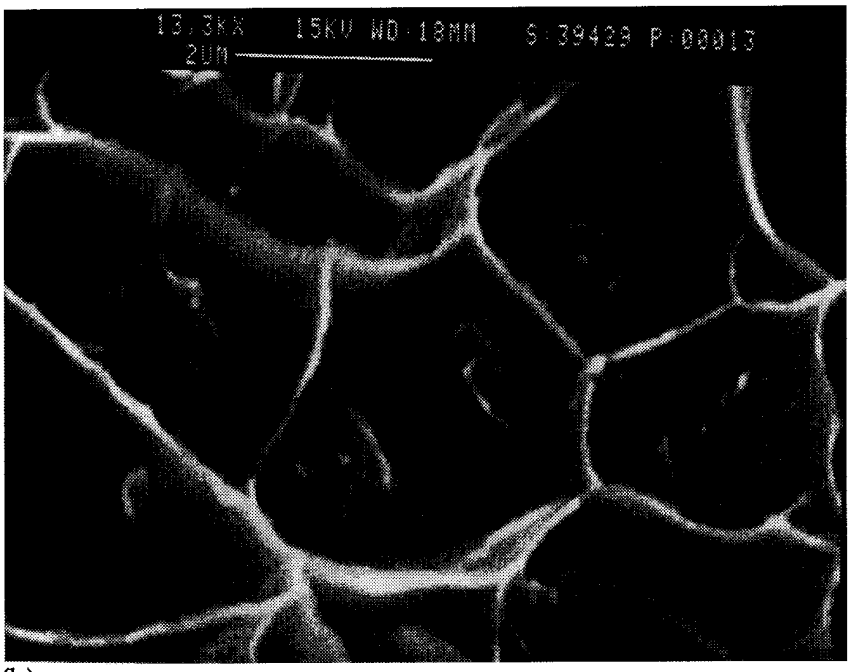
13.3KX 15KV WD-18MM S-39429 P-00013
2UM

(b)

(c)

Figure 5.9 Fracture surface of Al-4.5%Cu-1.2%Si composite at low magnification (a) and high magnification (b) in secondary electrons contrast and at high magnification (c) in backscattered electrons contrast.
(Photos 39429-12, 39429-13, 39429-14)

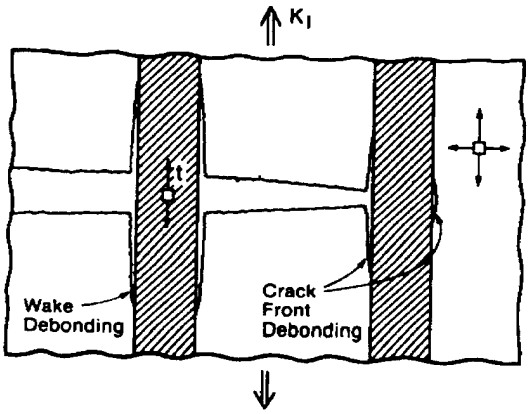

Figure 6.1 Interface delamination mechanical fuse crack deflection toughening mechanism in brittle matrix composites.

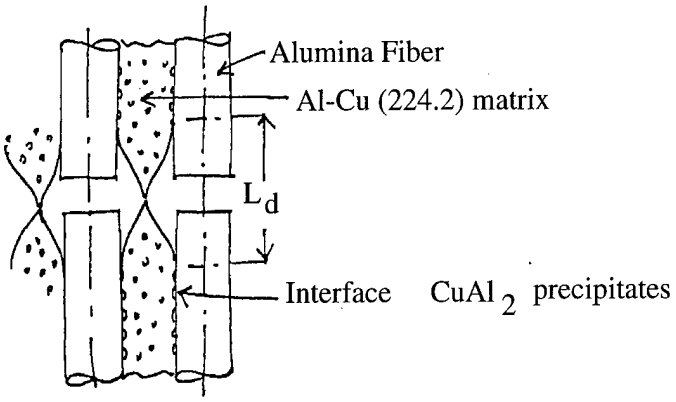

Figure 6.1 Interface delamination mechanical fuse crack deflection toughening mechanism in brittle matrix composites.

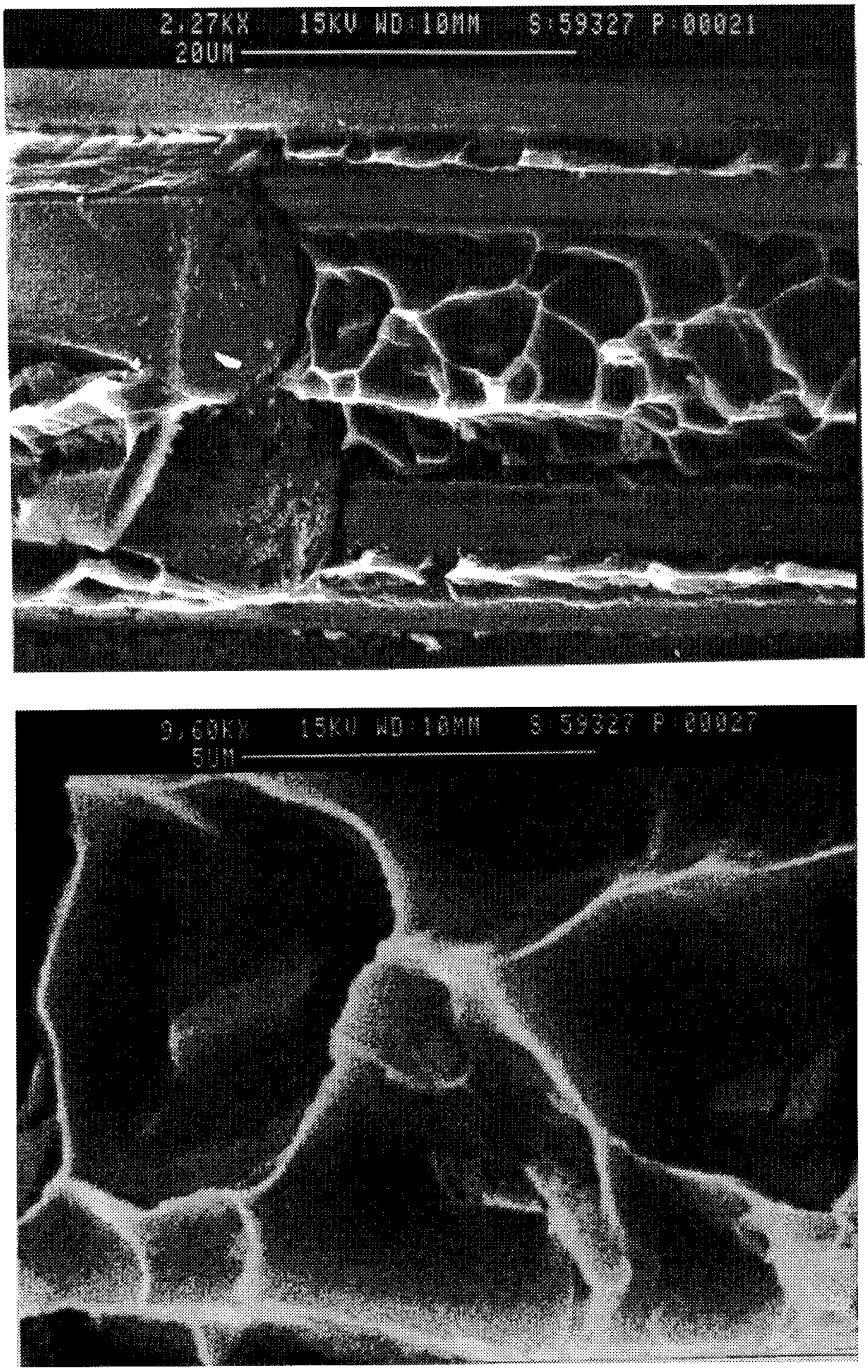

Figure 6.3 Fracture surface of the fiber-matrix interface on the matrix side after the specimen was tested in transverse mode and the fiber was torn-off. Matrix: Al-4.5%Cu. Heat treatment: 400C 30h.
(Photo 59327-27, 59327-21)

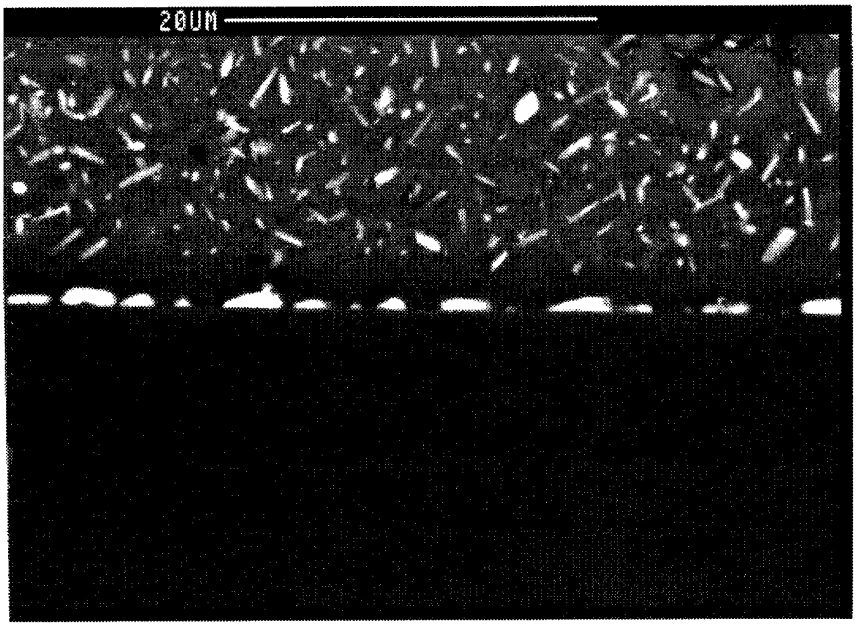

Figure 6.4 The CuAl2 precipitates on single crystal alumina substrate. (Photo 70993-11).

Figure 6.5 The example of CuAl2 precipitates on single crystal alumina substrate for which the contact angles were measured. (Photo 111093-27)

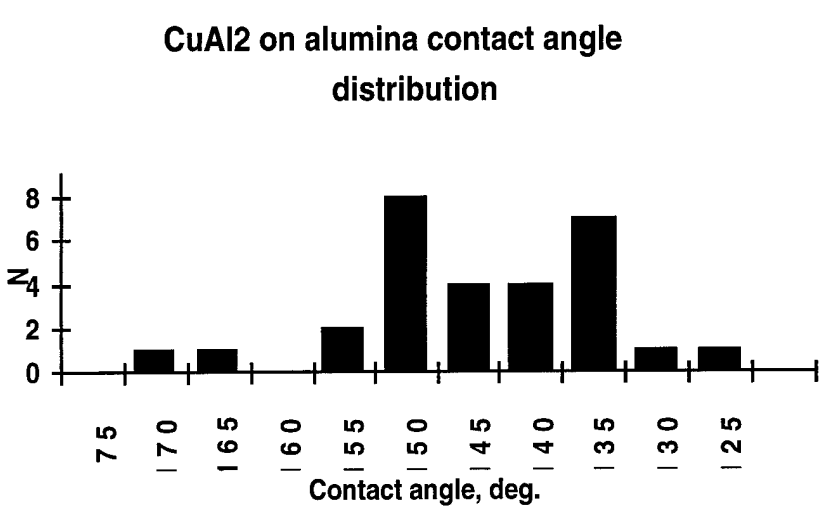

Figure 6.6 The distribution of contact angles between CuAl2 precipitates and alumina single crystal substrate. Matrix alloy: Al-4.5%Cu. Heat treatment: T7+ 150h at 400C.

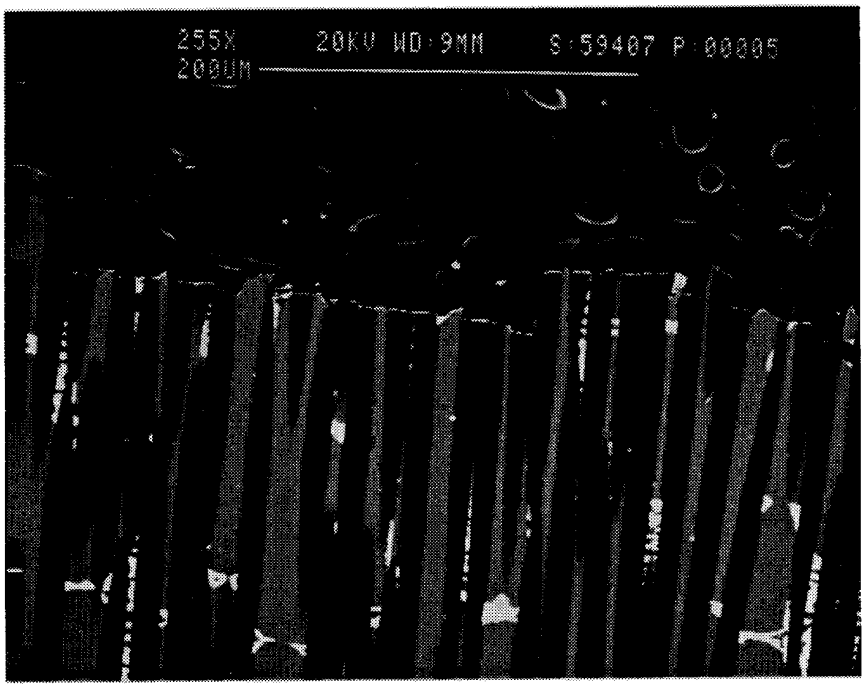

Figure 6.7 Cross-section of a fracture surface of T7 heat treated Al-224.2 matrix composite.
(Photo: 59407-5)

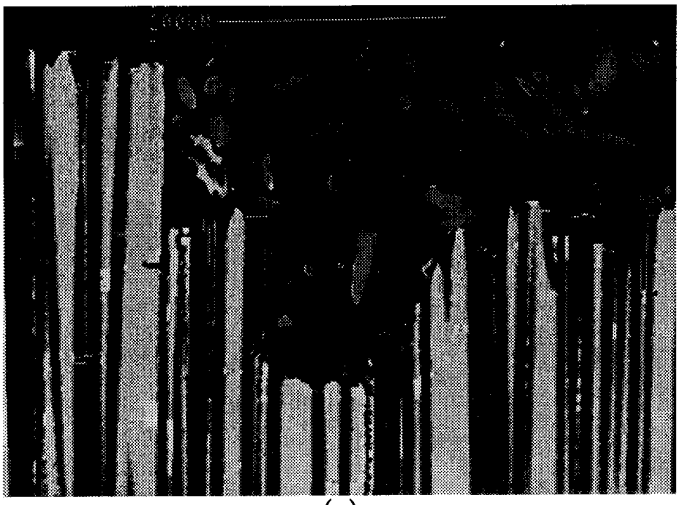

(a)

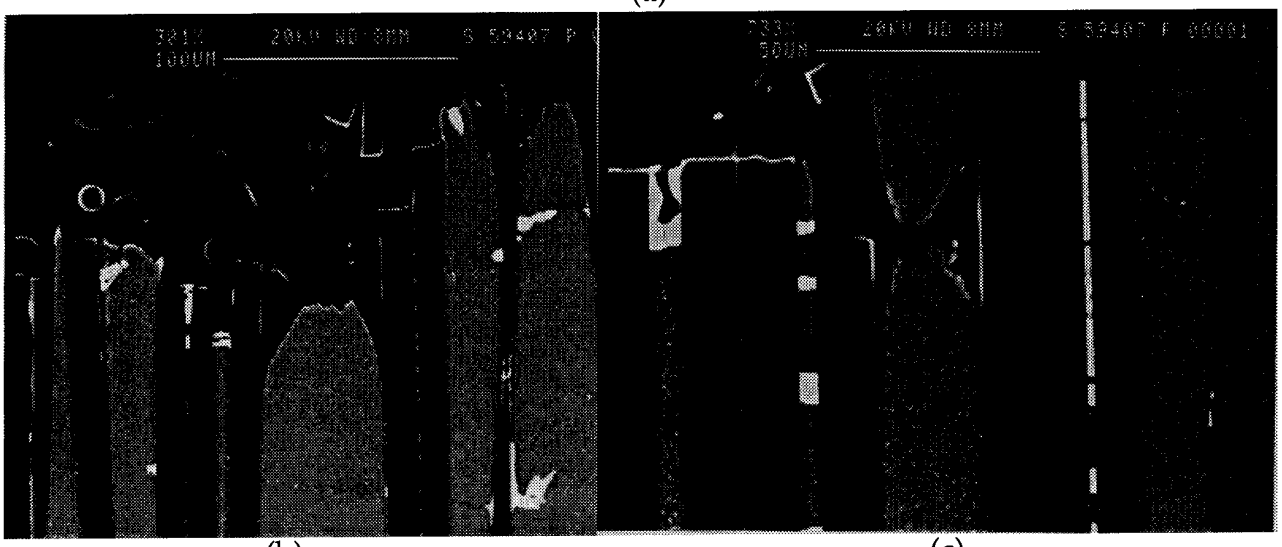

(b) (c)

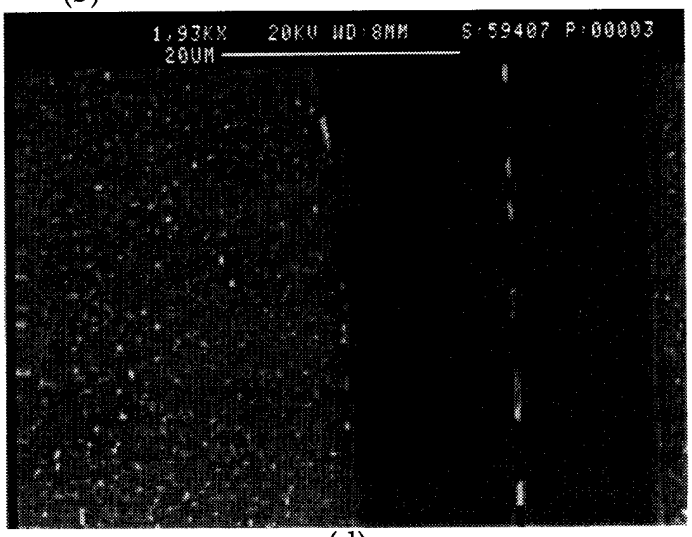

(d)

Figure 6.8 Cross-section of a fracture surface of Al-224.2 matrix composite. Heat treatment: T7 + 10h at 350C. (a) - low magnification view of the overall fracture; (b, c) - high magnification view of the plastically deforming matrix ligaments; (d) - high magnification view of debond area of the matrix ligaments from fiber. (Photos: 79419-6, 59407-2, 59407-1, 59407-3.)